

Supporting Information for

H₂ Addition to (Me⁴PCP)Ir(CO): Studies of the Isomerization Mechanism

Travis T. Lekich,[†] J. Brannon Gary,[‡] Sarina M. Bellows,[‡] Thomas R. Cundari,^{‡,*}, Louise M. Guard,[†] D. Michael Heinekey,^{‡,*}

[†]Department of Chemistry, University of Washington, Seattle, Washington 98195-1700.

[‡]Department of Chemistry, Center for Advanced Scientific Computing and Modeling (CASCaM), University of North Texas, P.O. Box 305070, Denton, Texas, 76203-5070.

^{*}Department of Chemistry & Biochemistry, Stephen F. Austin State University, Nacogdoches, TX 75962.

TABLE OF CONTENTS

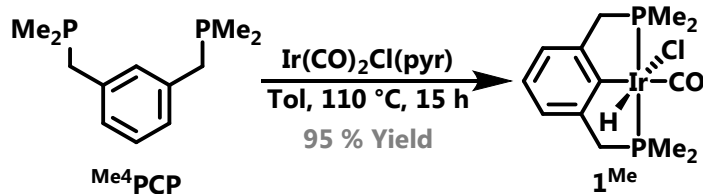
1. Experimental and Characterization	2
1.0 General Considerations	2
1.1 1^{Me} (Me ⁴ PCP)Ir(HCl)CO	3
1.2 2^{Me} (Me ⁴ PCP)Ir(CO)	6
1.3.0 trans-3^{Me} trans-(Me ⁴ PCP)Ir(H) ₂ CO	10
1.3.1 cis-3^{Me} cis-(Me ⁴ PCP)Ir(H) ₂ CO	14
1.4 4^{Me} : [(Me ⁴ PCP)Ir(H)(pyr)CO][OTf]	16
1.5 5^{Me} (Me ⁴ PCP)Ir(CO) ₂	19
1.6 6^{Me} (Me ⁴ PCP)Ir(PMe ₃)CO	22
1.7 trans-7^{Me} trans-(Me ⁴ PCP)Ir(H) ₂ (PMe ₃)	25
1.8 Crystal Structure of 2^{iPr} (iPr ⁴ PCP)Ir(CO)	27
1.9 Crystal Structure of trans-3^{tBu} trans-(tBu ⁴ PCP)Ir(H) ₂ (CO)	28
2. Attempts to Trap an Intermediate During cis/trans-3^{Me} Isomerization	29
3. KinetiC Analysis of the cis/trans-3^{Me} isomerization	30
3.0 Kinetics Summary	30
3.1 Eyring Analysis	30
3.2 Kinetics Experimental	30
3.3 Order Determination/Regression Analysis	31
4. Crystallographic Tables and Experimental.....	40
4.0 Crystallography Experimental	40
4.1 Crystallographic Tables	41
5. Computational Details	43
6. References	44

1. Experimental and Characterization

1.0 General Considerations. All manipulations and reactions used standard Schlenk and glovebox techniques under an argon or nitrogen atmosphere, unless otherwise stated. Glassware and diatomaceous earth were stored in an oven maintained at 140 °C for at least 24 h prior to use. All protio solvents were passed through activated alumina and activated 3Å molecular sieves prior to use. Deuterated solvents were dried over calcium hydride (CD_2Cl_2), or sodium (C_6D_6 , toluene-d₈, THF-d₈), and vacuum transferred prior to use. ^1H , $^{31}\text{P}\{^1\text{H}\}$, and $^{13}\text{C}\{^1\text{H}\}$ NMR spectra were recorded on a Bruker AV-300, AV-500, DRX-500, or AV-700 instrument. ^1H NMR and $^{13}\text{C}\{^1\text{H}\}$ NMR spectra were referenced to residual solvent signals.¹ $^{31}\text{P}\{^1\text{H}\}$ NMR spectra were referenced to an 85% H_3PO_4 standard. Elemental analysis was completed at the CENTC facility at the University of Rochester (funded by NSF CHE-0650456). $\text{Ir}(\text{CO})_2\text{Cl}(\text{pyr})$ and $^{\text{Me}4}\text{PCP}$ were synthesized as previously reported.²

1.1

1^{Me}: (^{Me₄}PCP)Ir(HCl)CO



1^{Me}: (^{Me₄}PCP)Ir(HCl)CO. Ir(CO)₂Cl(pyridine) (0.505g, 1.54 mmol) was added to a solution of ^{Me₄}PCP (0.350 g, 1.54 mmol) in toluene (15 mL). The addition was accompanied by effervescence, and an abundant precipitate. The mixture was heated at 110 °C for 15 h, resulting in a yellow solution. The solution was filtered through diatomaceous earth to remove trace particulates. The volatiles were removed under vacuum to afford a white powder. The white powder was triturated with pentane (3 x 1 mL), and then dried under vacuum to afford (^{Me₄}PCP)Ir(HCl)CO (0.704 g, 1.46 mmol, 95 % yield).

Table S1. Characterization data for **1^{Me}**.

Method	Data
¹ H NMR (300 MHz, CD ₂ Cl ₂):	7.07 (d; ³ J _{HH} = 7.5 Hz; 2H; Ar-H), 6.93 (t; ³ J _{HH} = 7.5 Hz; 1H; Ar-H), 3.80-3.30 (m; 4H; -CH ₂ -), 1.84 (m; 12H; P(CH ₃) ₂)
³¹ P{ ¹ H} NMR (121 MHz, CD ₂ Cl ₂):	2.23 (s)
¹³ C{ ¹ H} NMR (126 MHz, C ₆ D ₆):	178.4 (s; Ir-CO), 147.3 (s; C _{Ar}), 125.1 (s; C _{Ar}), 122.7 (s; C _{Ar}), 46.0 (vt; -(CH ₂)-), 17.7 (vt; P(CH ₃) ₂), 11.8 (vt; P(CH ₃) ₂)
IR (solution, CH ₂ Cl ₂ , cm ⁻¹)	v(CO) 2020, v(Ir-H) 2171
EA (C ₁₃ H ₂₀ ClIrOP ₂)	Calc: C 32.40; H 4.18 Found: C 33.57; H 4.12

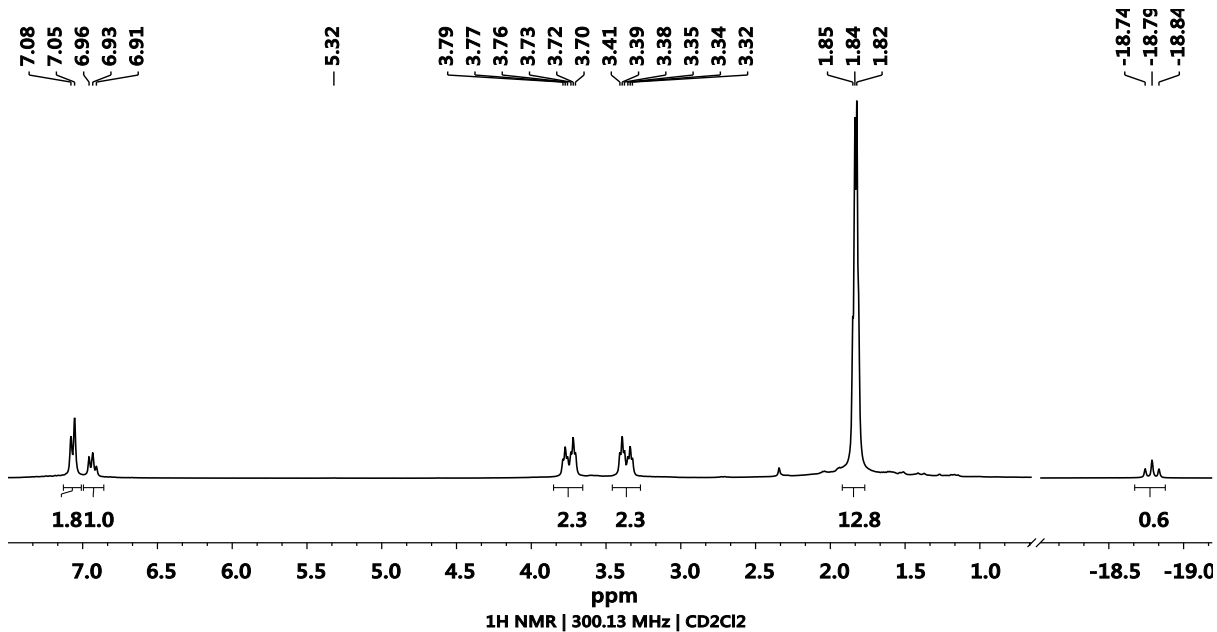


Figure S1. ¹H NMR spectrum of (^{Me₄PCP})Ir(HCl)CO (**1^{Me}**) in CD₂Cl₂. ¹H NMR (300 MHz, CD₂Cl₂): δ 7.07 (d; ³J_{HH} = 7.5 Hz; 2H; Ar-H), 6.93 (t; ³J_{HH} = 7.5 Hz; 1H; Ar-H), 3.80-3.30 (m; 4H, Ar(-CH₂-)), 1.84 (m; 12H, -P(CH₃)), -18.8 (t; ²J_{HP} = 13.8 Hz; 1H; Ir-H).

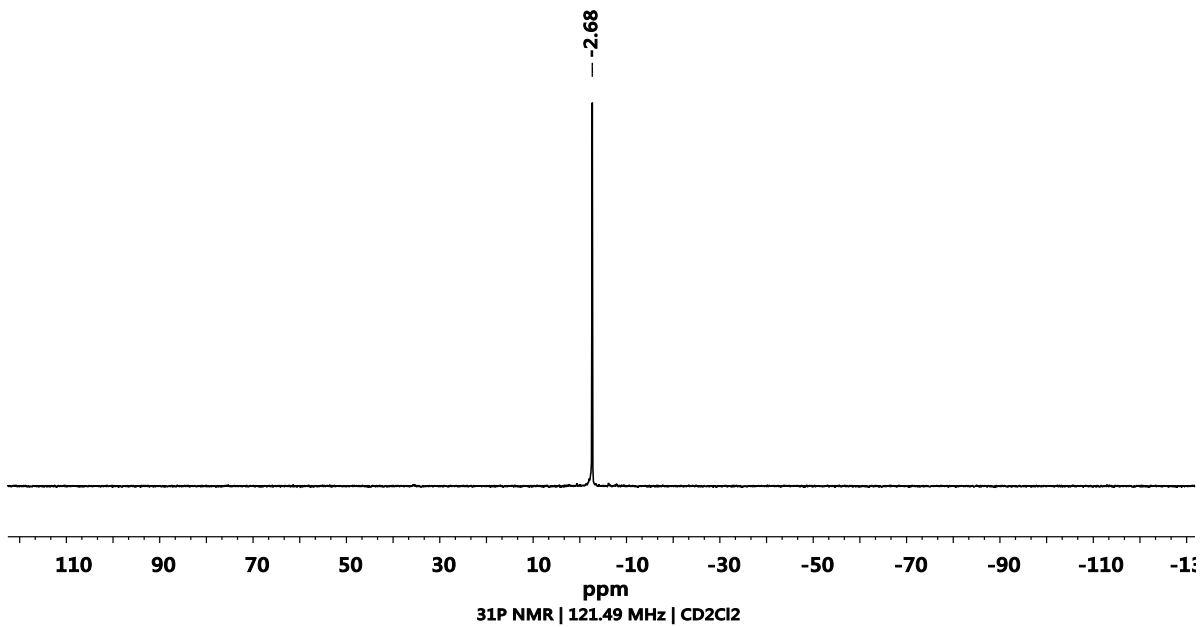


Figure S2. ³¹P{¹H} NMR spectrum of (^{Me₄PCP})Ir(HCl)CO (**1^{Me}**) in CD₂Cl₂. ³¹P{¹H} NMR (121 MHz, CD₂Cl₂): δ -2.68.

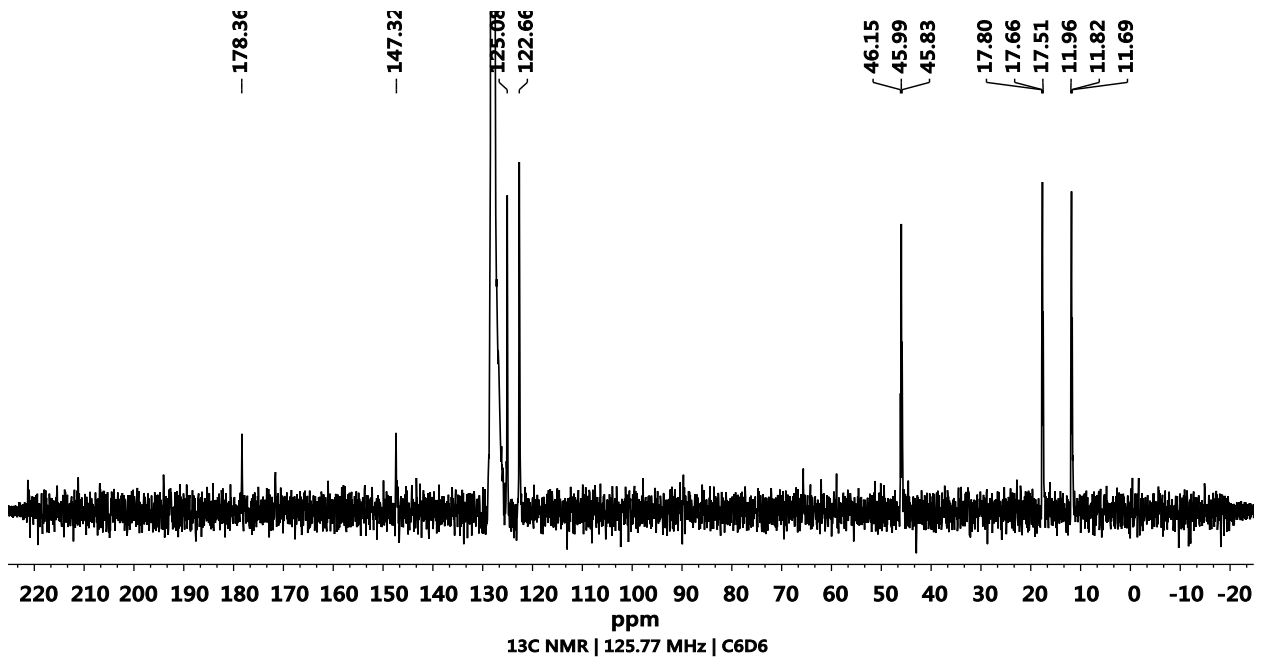
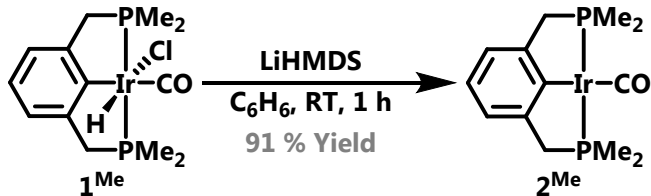


Figure S3. $^{13}\text{C}\{^1\text{H}\}$ NMR spectrum ($^{\text{Me}4}\text{PCP}$)Ir(HCl)CO (**I^{Me}**) in C₆D₆. $^{13}\text{C}\{^1\text{H}\}$ NMR (126 MHz, C₆D₆): δ 178.4 (s; Ir-CO), 147.3 (s; C_{Ar}), 125.1 (s; C_{Ar}), 122.7 (s; C_{Ar}), 46.0 (vt; -(CH₂)-), 17.7 (vt; P(CH₃)), 11.8 (vt; P(CH₃)).

1.2

2^{Me}: (^{Me⁴}PCP)Ir(CO)



2^{Me}: (^{Me⁴}PCP)Ir(CO). (^{Me⁴}PCP)Ir(HCl)(CO) (**1^{Me}**) (0.22 g, 0.46 mmol) and KHMDS (0.092 g, 0.46 mmol) were stirred in benzene for 1 hour at room temperature. The mixture was filtered through diatomaceous earth, and then the solvent was removed under vacuum to afford (^{Me⁴}PCP)Ir(CO) (0.188 g, 0.42 mmol, 91 % yield). X-ray diffraction quality crystals of (^{Me⁴}PCP)Ir(CO) were grown from slow evaporation of a concentrated solution of (^{Me⁴}PCP)Ir(CO) in pentane at -35 °C over 7 days.

Table S2. Characterization data for **2^{Me}**.

Method	Data
¹H NMR (300 MHz, C ₆ D ₆):	7.17 (d; ³ J _{HH} = 7.3 Hz; 2H; Ar-H), 7.09 (t; ³ J _{HH} = 7.3 Hz; 1H; Ar-H), 3.07 (vt; 4H; Ar(-CH ₂ -)), 1.84 (vt; 12H; -P(CH ₃))
³¹P{¹H} NMR (121 MHz, C ₆ D ₆):	17.1 (s)
¹³C{¹H} NMR (126 MHz, C ₆ D ₆):	196.8 (m; Ir-CO) 180.8 (m; C _{Ar}) 126.3 (m; C _{Ar}) 121.3 (m; C _{Ar}) 47.7 (vt, -(CH ₂)-) 16.9 (vt, -P(CH ₃))
IR (solution, C ₆ D ₆ , cm ⁻¹)	v(CO) 1933
EA (C ₁₃ H ₁₉ IrOP ₂)	Calc: C 35.05; H 4.03 Found C 34.67; H 4.04

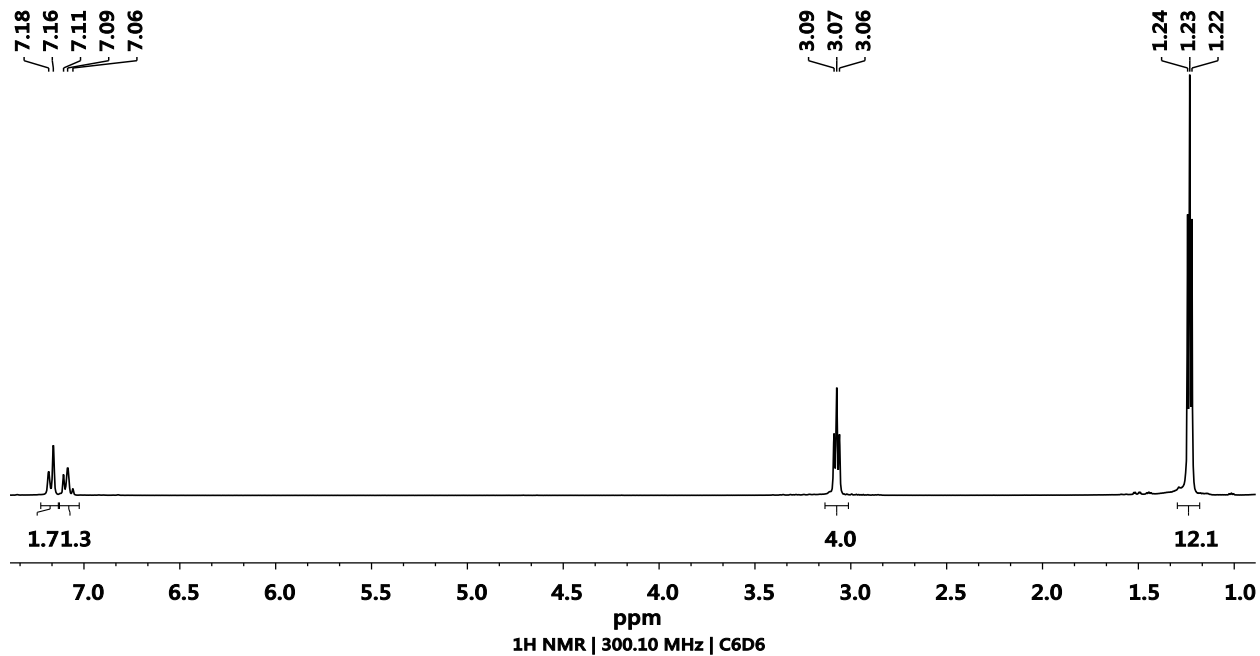


Figure S4. ${}^1\text{H}$ NMR spectrum of $({}^{\text{Me}4}\text{PCP})\text{Ir}(\text{CO}) (2^{\text{Me}})$ in C_6D_6 . ${}^1\text{H}$ NMR (300 MHz, C_6D_6): δ 7.17 (d; ${}^3J_{\text{HH}} = 7.3$ Hz; 2H; Ar-H), 7.09 (t; ${}^3J_{\text{HH}} = 7.3$ Hz; 1H; Ar-H), 3.07 (vt; 4H; Ar(- CH_2 -)), 1.84 (vt; 12H; - $\text{P}(\text{CH}_3)$).

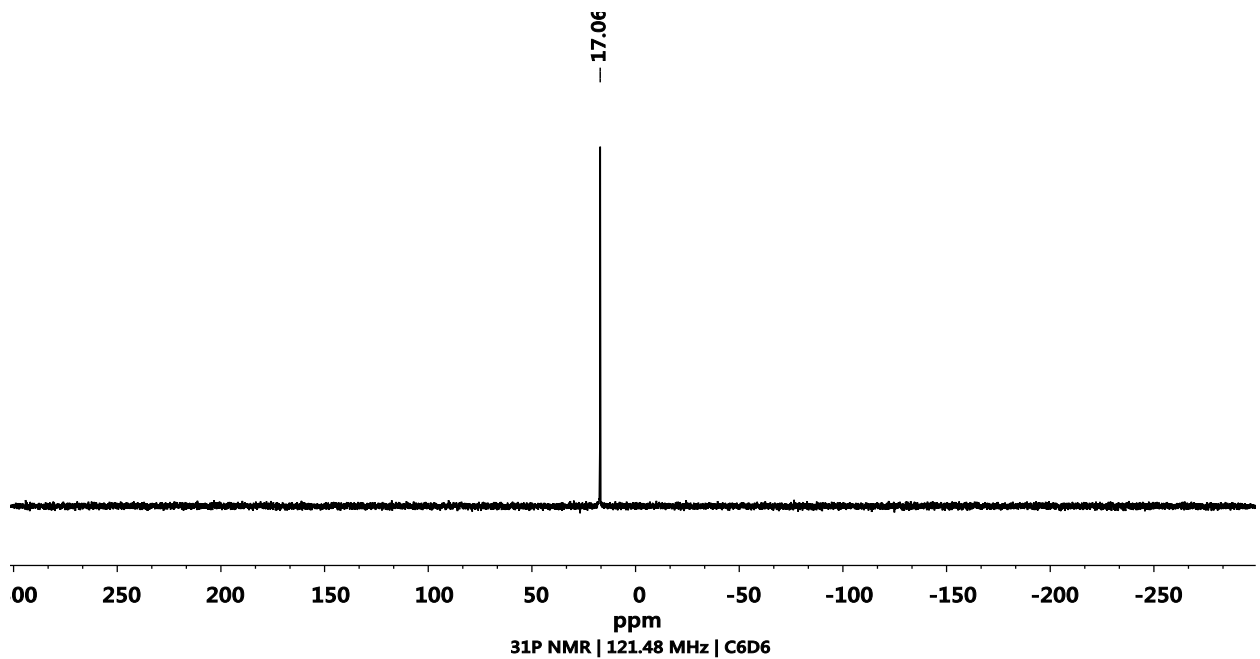


Figure S5. ${}^{31}\text{P}\{{}^1\text{H}\}$ NMR spectrum of $({}^{\text{Me}4}\text{PCP})\text{Ir}(\text{CO}) (2^{\text{Me}})$ in C_6D_6 . ${}^{31}\text{P}\{{}^1\text{H}\}$ NMR (121.5 MHz, C_6D_6): δ 17.1.

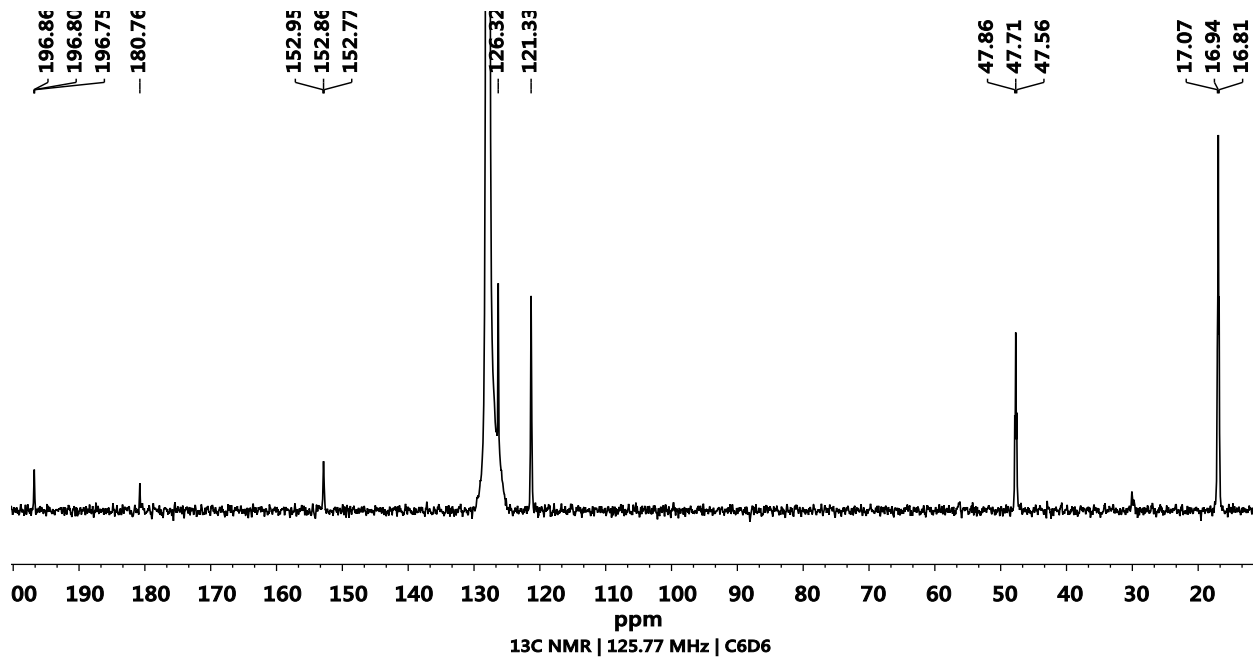


Figure S6. $^{13}\text{C}\{^1\text{H}\}$ NMR spectrum of $(^{\text{Me}_4}\text{PCP})\text{Ir}(\text{CO})$ (**2^{Me}**) in C₆D₆. $^{13}\text{C}\{^1\text{H}\}$ NMR (126 MHz, C₆D₆): δ 196.8 (m; Ir-CO), 180.8 (m; C_{Ar}), 152.9 (m; C_{Ar}), 126.3 (m; C_{Ar}), 121.3 (m; C_{Ar}), 47.7 (vt, -(CH₂)-), 16.9 (vt, -P(CH₃)).

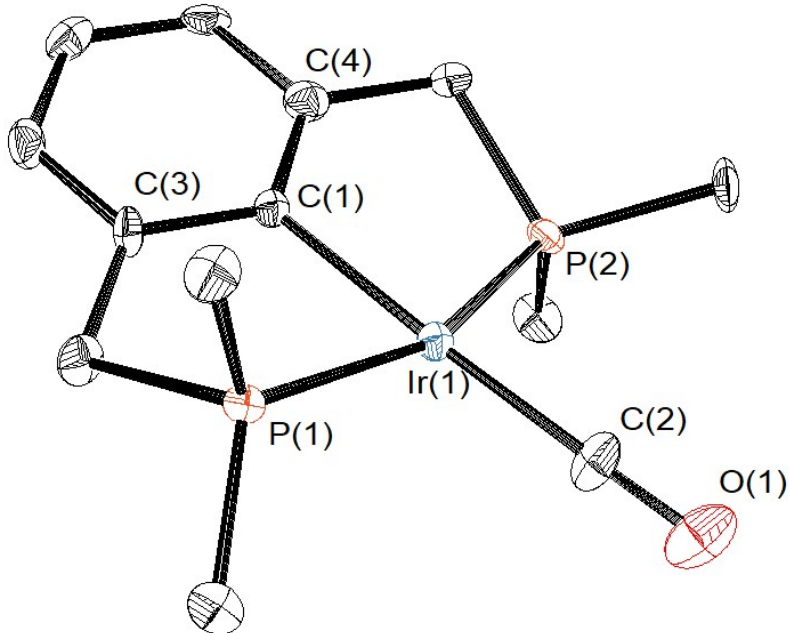


Figure S7. ORTEP⁴ of (^{Me4}PCP)Ir(CO) (**2^{Me}**) shown with thermal ellipsoids at 50% probability.
Hydrogen atoms are omitted for clarity.

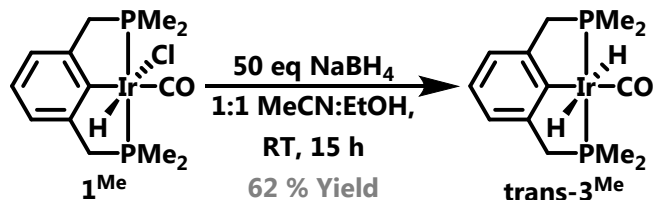
Table S3. Selected Bond Lengths and Angles for (^{Me4}PCP)Ir(CO) (2^{Me}**)**

A ^a		B ^a	
Bond (Å) or Angle (°)	Value	Bond (Å) or Angle (°)	Value
Ir(1)-C(1)	2.111 (3) Å	Ir(1)-C(1)	2.122 (3) Å
Ir(1)-C(2)	1.868 (7) Å	Ir(1)-C(2)	1.881 (7) Å
Ir(I)-O(1)	3.015 (6) Å	Ir(I)-O(1)	3.013 (6) Å
Ir(1)-P(1)	2.2871 (17) Å	Ir(1)-P(1)	2.2754 (17) Å
Ir(1)-P(2)	2.2787 (17) Å	Ir(1)-P(2)	2.2756 (18) Å
C(2)-O(1)	1.148 (9) Å	C(2)-O(1)	1.132 (9) Å
P(1)-Ir(1)-P(2)	160.49 (6) °	P(1)-Ir(1)-P(2)	162.61 (7) °
C(1)-Ir(1)-C(2)	178.0 (2) °	C(1)-Ir(1)-C(2)	176.1 (2) °
C(3)-C(1)-Ir(1)-P(1)	15.7 (3) °	C(3)-C(1)-Ir(1)-P(1)	11.0 (2) °
C(4)-C(1)-Ir(1)-P(2)	17.8 (3) °	C(4)-C(1)-Ir(1)-P(2)	14.7 (3) °

^a(^{Me4}PCP)Ir(CO) (**2^{Me}**) crystallized with two molecules in the asymmetric unit, conformations labeled A and B.

1.3.0

trans-3^{Me}: trans-(^{Me⁴}PCP)Ir(H)₂(CO)



trans-3^{Me}: trans-(^{Me⁴}PCP)Ir(H)₂(CO). NaBH₄ (0.416 g, 11.0 mmol) and (^{Me⁴}PCP)Ir(HCl)CO (0.106 g, 0.220 mmol) were stirred in 1:1 ethanol (10 mL): acetonitrile (10 mL) in a 50 mL Schlenk tube. The solvent was removed under vacuum, resulting in a white solid. The solid was extracted with benzene and the mixture was filtered through diatomaceous earth. The solvent was removed under vacuum to give a white solid, which was washed with cold (-35 °C) pentane to afford (^{Me⁴}PCP)Ir(H)₂(CO) (0.061g, 0.136 mmol, 62 % yield).

Table S4. Characterization data for **trans-3^{Me}**.

Method	Data
¹ H NMR	7.09 (m; 3H; Ar-H), (300 MHz, C ₆ D ₆): 3.14 (vt; 4H; Ar(-CH ₂ -)), 1.42 (vt; 12H, -P(CH ₃)), -9.23 (t; ² J _{HP} = 16.4; 2H; Ir-H)
³¹ P{ ¹ H} NMR	-6.08 (s) (121 MHz, C ₆ D ₆):
¹³ C{ ¹ H} NMR	179.8 (s; Ir-CO) (126 MHz, Tol-d ₈): 153.6 (s; C _{Ar}) 146.2 (s; C _{Ar}), 123.1 (s; C _{Ar}), 122.0 (s; C _{Ar}), 50.3 (vt; -(CH ₂)-), 20.9 (vt; P(CH ₃))
IR (solution, C ₆ D ₆ , cm ⁻¹)	v(CO) 1992, v(Ir-H) 1722
EA (C ₁₃ H ₂₁ IrOP ₂)	Calcd: C 34.89; H 4.73 Found C 35.78; H 4.77

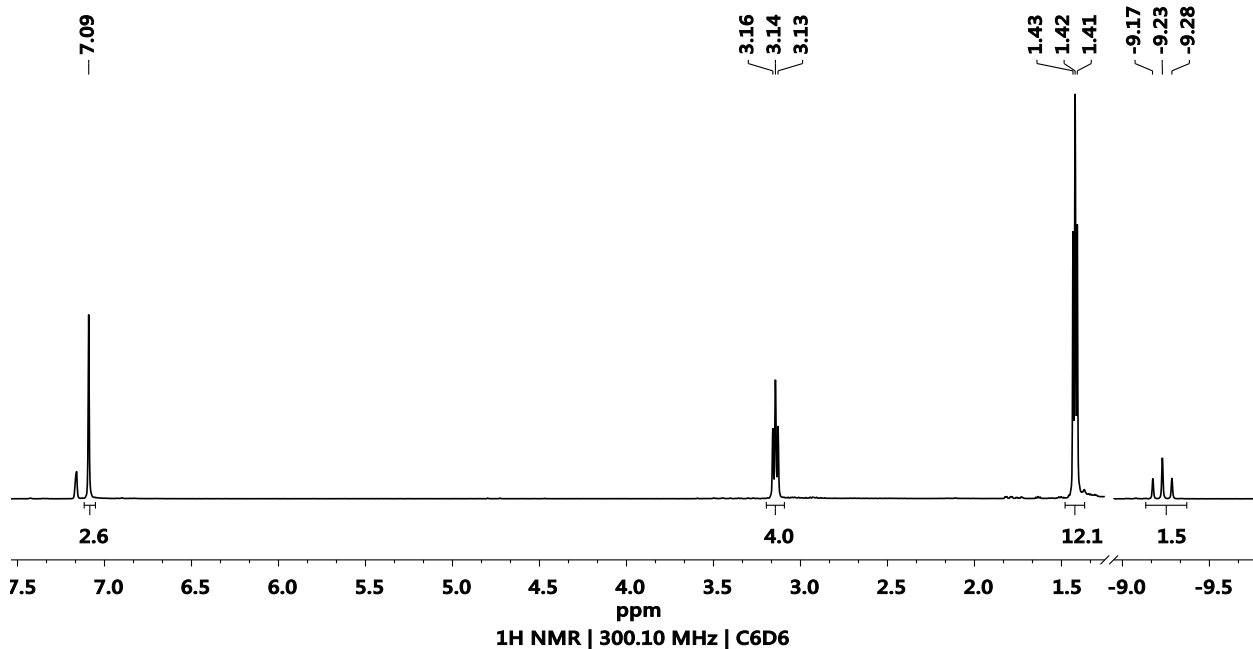


Figure S8. ^1H NMR spectrum of trans-($^{\text{Me}4}\text{PCP}$)Ir(H)₂(CO) (**trans-3^{Me}**) in C₆D₆. ^1H NMR (300 MHz, C₆D₆): δ 7.09 (m; 3H; Ar-H), 3.14 (vt; 4H; Ar(-CH₂-)), 1.42 (vt; 12H, -P(CH₃)), -9.23 (t; $^2J_{\text{HP}} = 16.4$; 2H; Ir-H).

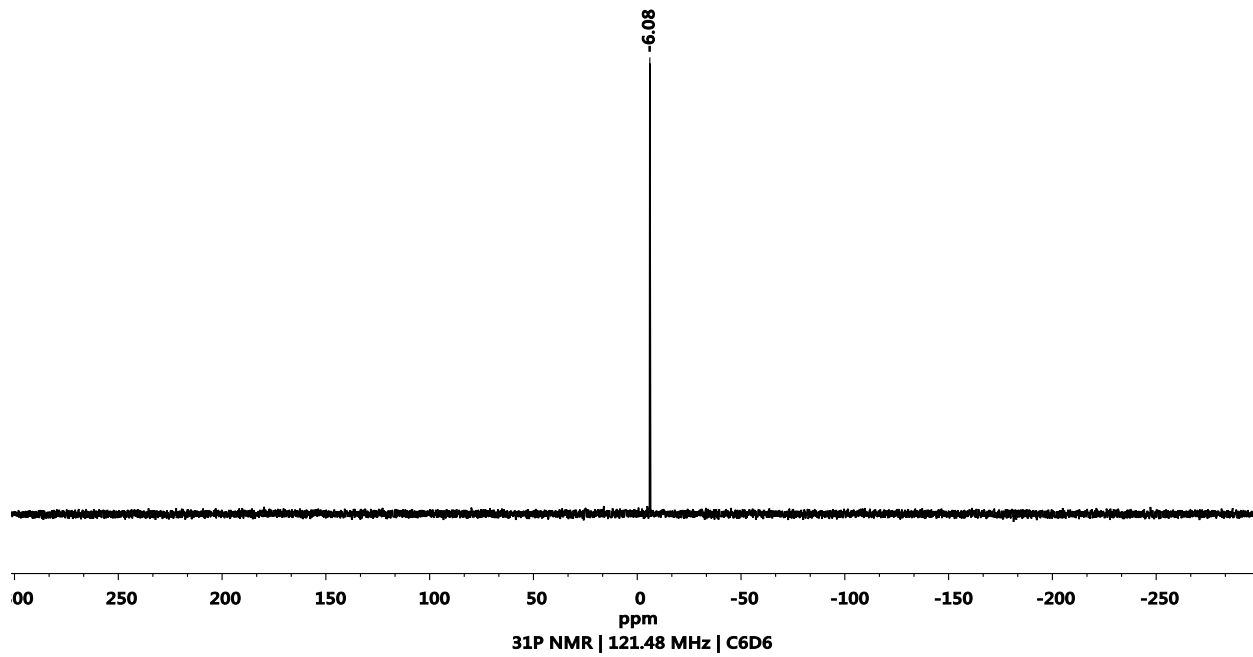


Figure S9. $^{31}\text{P}\{^1\text{H}\}$ NMR spectrum of trans-($^{\text{Me}4}\text{PCP}$)Ir(H)₂(CO) (**trans-3^{Me}**) in C₆D₆. $^{31}\text{P}\{^1\text{H}\}$ NMR (121.5 MHz, C₆D₆): δ -6.08.

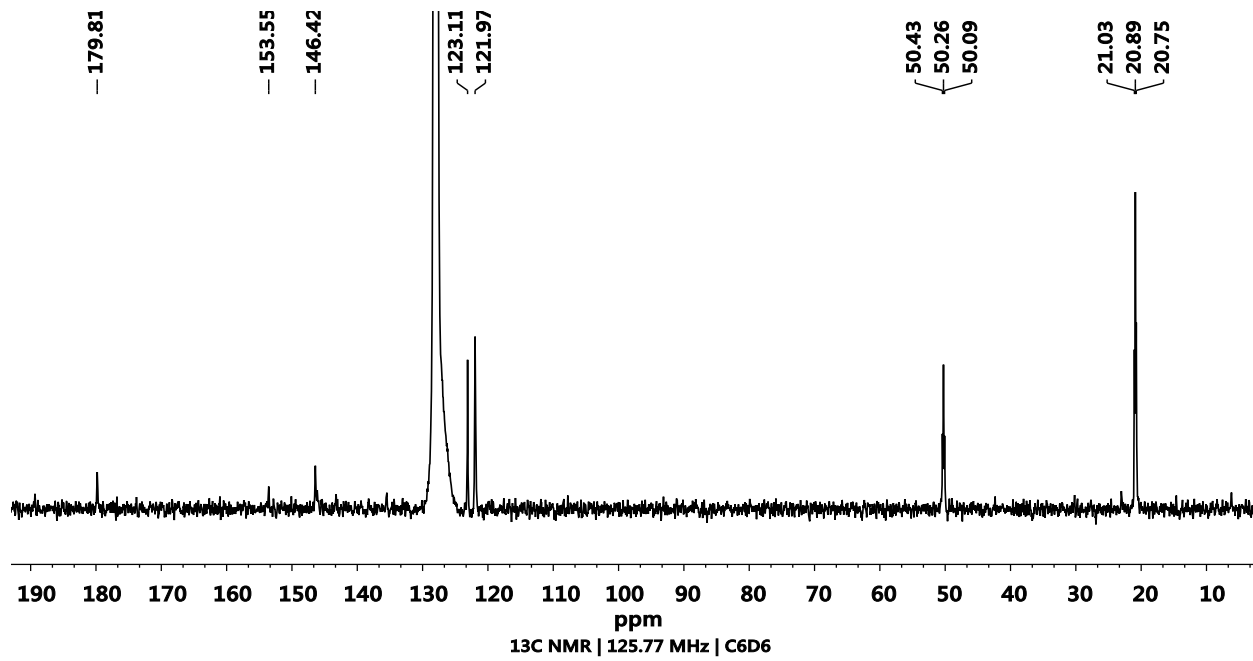


Figure S10. $^{13}\text{C}\{^1\text{H}\}$ NMR spectrum of trans-(Me_4PCP)Ir(H)₂(CO) (**trans-3^{Me}**) in C₆D₆. $^{13}\text{C}\{^1\text{H}\}$ NMR (126 MHz, C₆D₆): δ 179.8 (s; Ir-CO), 153.6 (s; C_{Ar}), 146.2 (s; C_{Ar}), 123.1 (s; C_{Ar}), 122.0 (s; C_{Ar}), 50.3 (vt; - (CH₂)-), 20.9 (vt; P(CH₃)).

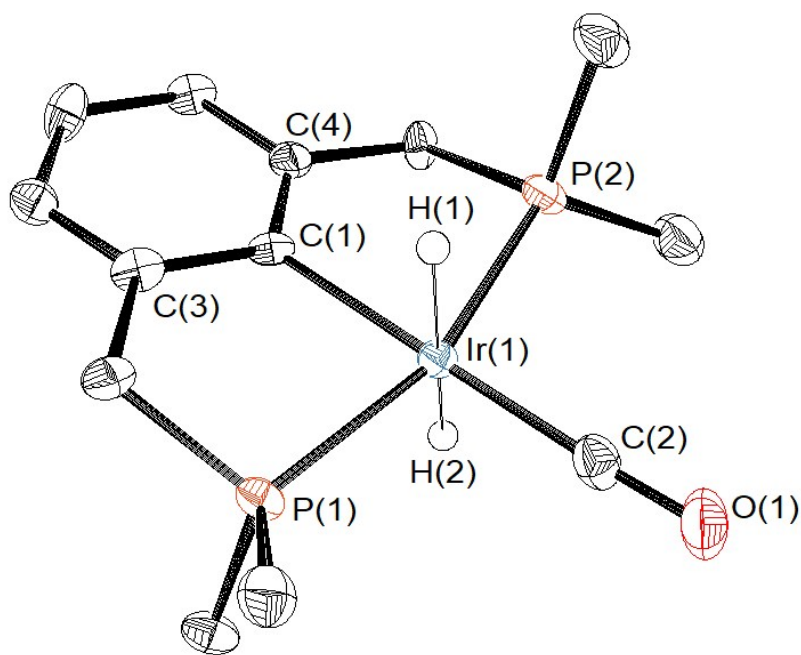


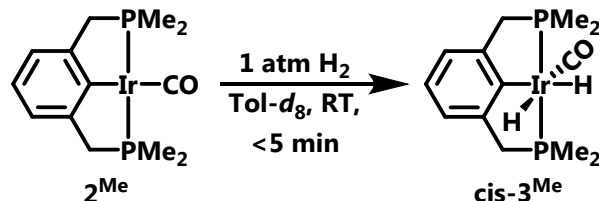
Figure S11. ORTEP⁴ of *trans*-(^{Me}₄PCP)Ir(H)₂(CO) (**trans-3^{Me}**) shown with thermal ellipsoids at 50% probability. The hydrogen atoms, except for the hydrides, are omitted for clarity.

Table 5. Selected bond lengths and angle for the crystal structure of *trans*-(^{Me}₄PCP)Ir(H)₂(CO) (**trans-3^{Me}**), shown in **Figure S11**.

trans-(^{Me}₄PCP)Ir(H)₂(CO)	
Bond (Å) or Angle (°)	Value
Ir(1)-C(1)	1.877 (10) Å
Ir(1)-P(1)	2.293 (2) Å
Ir(1)-P(2)	2.287 (2) Å
Ir(1)-C(2)	1.877 (10) Å
Ir(1)-O(1)	3.046 (2) Å
C(2)-O(1)	1.170 (12) Å
P(1)-Ir(1)-P(2)	161.19 (9) °
C(1)-Ir(1)-C(2)	178.1 (3) °
C(3)-C(1)-Ir(1)-P(1)	15.2 (6) °
C(4)-C(1)-Ir(1)-P(2)	14.2 (6) °

1.3.1

cis-3^{Me}: cis-(^{Me⁴}PCP)Ir(H)₂(CO)



cis-3^{Me}: cis-(^{Me⁴}PCP)Ir(H)₂(CO). A J-Young NMR tube was charged with (^{Me⁴}PCP)Ir(CO) (**2^{Me}**) (ca. 5 mg, 0.01 mmol) and C₆D₆. The solution was degassed, then introduced to 1 atm H₂. The J-Young NMR tube was vigorously shaken for 20 seconds. ¹H and ³¹P{¹H} NMR spectra were recorded ca. 5 minutes after H₂ addition. To obtain the IR spectrum, **2^{Me}** was introduced to 1 atm H₂ as described then immediately transferred to a solution IR cell under a flow of H₂. The ν(*Ir-H*) peaks were assigned by comparing the spectra of **cis-3^{Me}** and **cis-3^{Me-d2}** (cis-(^{Me⁴}PCP)Ir(D)₂(CO)). **cis-3^{Me-d2}** was synthesized by adding 1 atm D₂ to **2^{Me}** and C₆D₆ in a J-Young NMR tube.

Table S6. Characterization data for **cis-3^{Me}**.

Method	Data
¹ H NMR (300 MHz, C ₆ D ₆):	7.16 (m; 3H; <i>Ar</i>), 3.18 (vt; 4H; -CH ₂ -), 1.40 (vt; 6H; P(CH ₃) ₂), 1.36 (vt; 6H; P(CH ₃) ₂), -9.85 (t; ² J _{HP} = 19.2 Hz; 1H), -11.0 (t; ² J _{HP} = 12.4 Hz; ² J _{HH} = 3.0 Hz; 1H)
³¹ P{ ¹ H} NMR (121 MHz, C ₆ D ₆):	-12.3 (s)
IR (solution, C ₆ D ₆ , cm ⁻¹)	ν(CO) 2010, ν(<i>Ir-H</i>) 2055, 1950

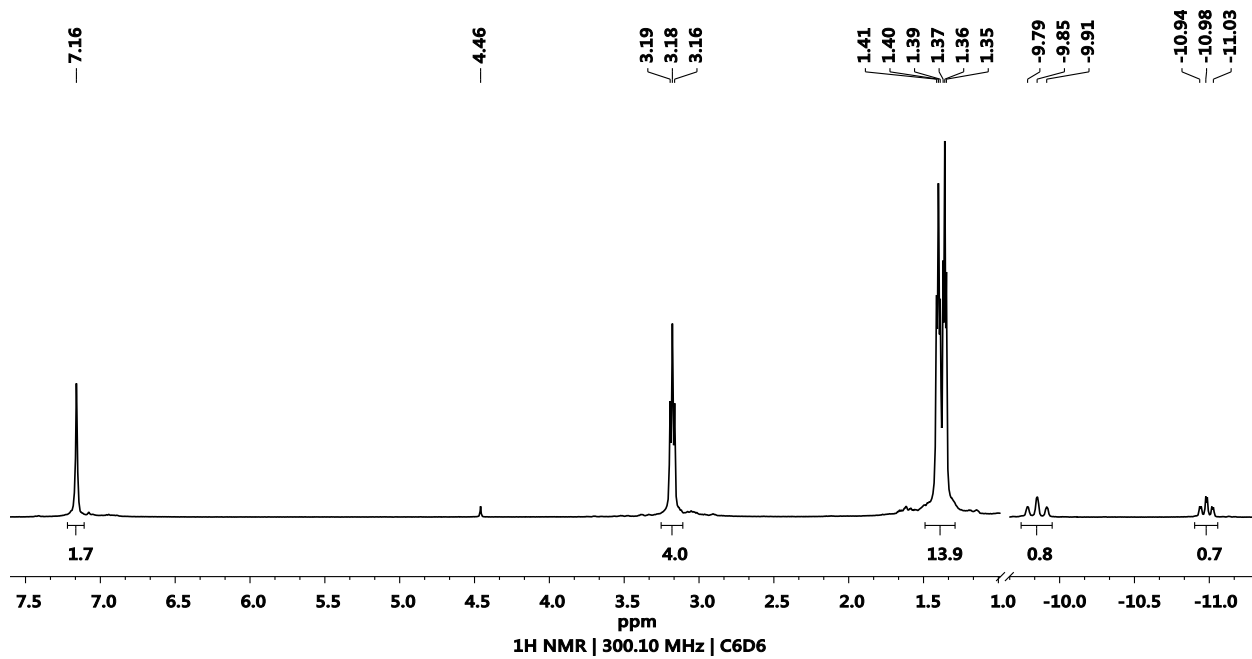


Figure S12. ^1H NMR spectrum of $\text{cis}-(\text{Me}^4\text{PCP})\text{Ir}(\text{H})_2(\text{CO})$ (**cis-3^{Me}**) in C_6D_6 with a minor amount of **trans-3^{Me}** and H_2 . ^1H NMR (300 MHz, C_6D_6): 7.16 (m; 3H; *Ar*), 3.18 (vt; 4H; $-\text{CH}_2-$), 1.40 (vt; 6H; $\text{P}(\text{CH}_3)_2$), 1.36 (vt; 6H; $\text{P}(\text{CH}_3)_2$), -9.85 (t; $^2J_{\text{HP}} = 19.2$ Hz; 1H), -11.0 (t; $^2J_{\text{HP}} = 12.4$ Hz; $^2J_{\text{HH}} = 3.0$ Hz 1H).

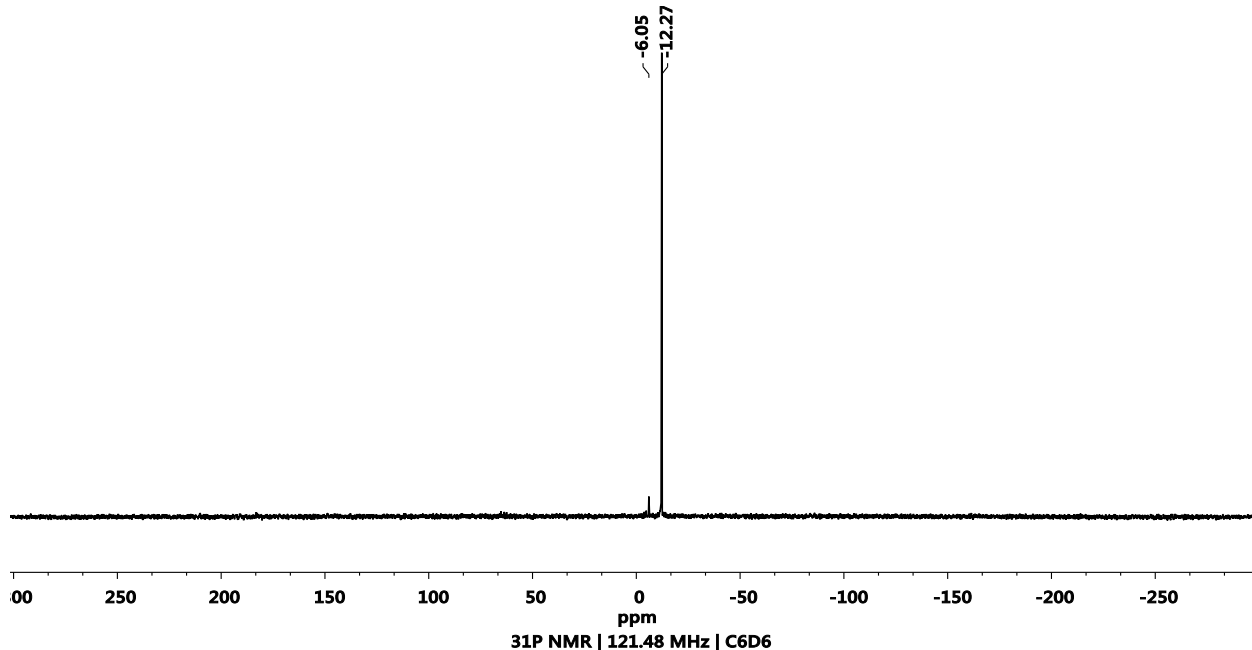
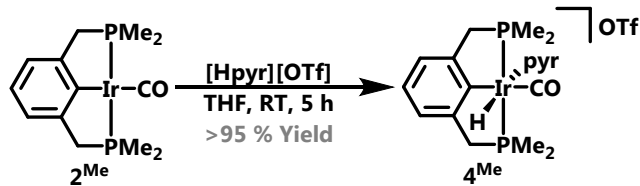


Figure S13. $^{31}\text{P}\{^1\text{H}\}$ NMR spectrum of $\text{cis}-(\text{Me}^4\text{PCP})\text{Ir}(\text{H})_2(\text{CO})$ (**cis-3^{Me}**) in C_6D_6 with a minor amount of **trans-3^{Me}**. $^{31}\text{P}\{^1\text{H}\}$ NMR (121 MHz, C_6D_6): δ -12.3.

1.4

4^{Me}: [(^{Me₄}PCP)Ir(H)(pyr)CO][OTf]



4^{Me}: [(^{Me₄}PCP)Ir(H)(pyr)CO][OTf]. (^{Me₄}PCP)Ir(CO) (**2^{Me}**) (42 mg, 0.09 mmol) and pyridinium triflate (15 mg, 0.09 mmol) were stirred in THF (1 mL) in a scintillation vial for 5 h. The precipitate was removed by filtration through diatomaceous earth, then the volatiles were removed under vacuum. The resulting off-white solid was washed with benzene, then the volatiles were removed under vacuum to afford [(^{Me₄}PCP)Ir(H)(pyr)CO][OTf] (54 mg, 0.08 mmol, 95 % yield).

Table S7. Characterization data for **4^{Me}**.

Method	Data
¹ H NMR (300 MHz, CD ₂ Cl ₂):	8.09 (d; ³ J _{HH} = 5.2 Hz; 2H; C ₅ H ₅ N), 7.89 (t; ³ J _{HH} = 7.45 Hz; 1H; C ₅ H ₅ N), 7.32 (app t; 2H; C ₅ H ₅ N), 7.17 (m; 2H; Ar-H), 7.09 (m; 1H; Ar-H), 3.55-3.32 (m; 4H; Ar(-CH ₂ -)), 1.89 (vt; 6H; -P(CH ₃) ₂), 1.31 (vt; 6H; -P(CH ₃) ₂), -19.4 (t; ³ J _{HH} = 14.2 Hz 1H; Ir-H)
³¹ P{ ¹ H} NMR (121 MHz, CD ₂ Cl ₂):	1.07 (s)
¹³ C{ ¹ H} NMR (176 MHz, CD ₂ Cl ₂):	177.3 (s; Ir-CO), 157.9 (s; C _{Ar}), 154.1 (s; C _{Ar}), 147.9 (t; ³ J _{CP} = 7.5 Hz; C _{Ar}), 140.1 (s; C _{Ar}), 128.0 (s; C _{Ar}), 127.3 (s; C _{Ar}), 124.6 (t; ³ J _{CP} = 8.6 Hz; C _{Ar}), 45.5 (vt; -(CH ₂)-), 19.0 (vt; P(CH ₃)), 16.1 (vt; P(CH ₃))
IR (solution, CD ₂ Cl ₂ , cm ⁻¹)	v(CO) 2032, v(Ir-H) 2183
EA	Calcd: C 33.83; N 2.08; H 3.74 Found: C 33.82; N 2.11; H 3.57

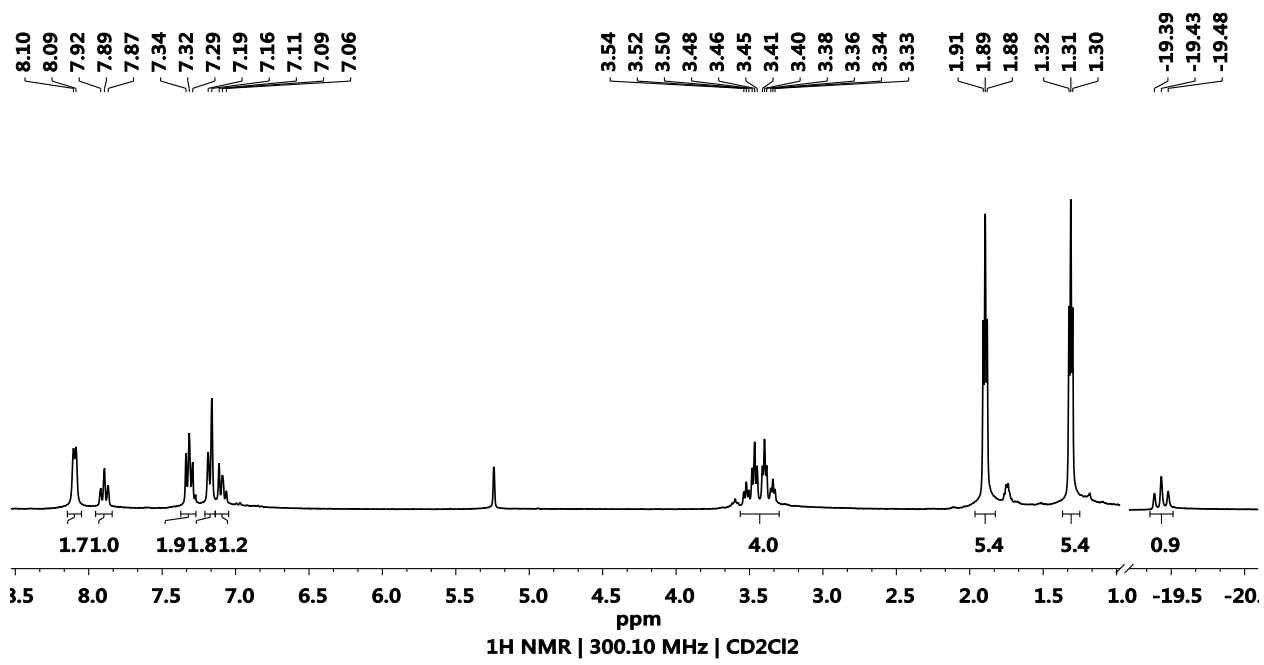


Figure S14. ^1H NMR spectrum of $(^{\text{Me}4}\text{PCP})\text{Ir}(\text{H})(\text{pyr})\text{CO}[\text{OTf}]$ (**4^{Me}**) in CD_2Cl_2 . ^1H NMR (300 MHz, CD_2Cl_2): δ 8.09 (d; $^3J_{\text{HH}}$ 5.2 Hz; 2H; $\text{C}_5\text{H}_5\text{N}$), 7.89 (t; $^3J_{\text{HH}}$ = 7.45 Hz; 1H; $\text{C}_5\text{H}_5\text{N}$), 7.32 (app t; 2H; $\text{C}_5\text{H}_5\text{N}$), 7.17 (m; 2H; Ar-H), 7.09 (m; 1H; Ar-H), 3.55-3.32 (m; 4H; Ar(- CH_2 -)), 1.89 (vt; 6H; - $\text{P}(\text{CH}_3)_2$), 1.31 (vt; 6H; - $\text{P}(\text{CH}_3)_2$), -19.4 (t; $^3J_{\text{HH}}$ = 14.2 Hz 1H; Ir-H).

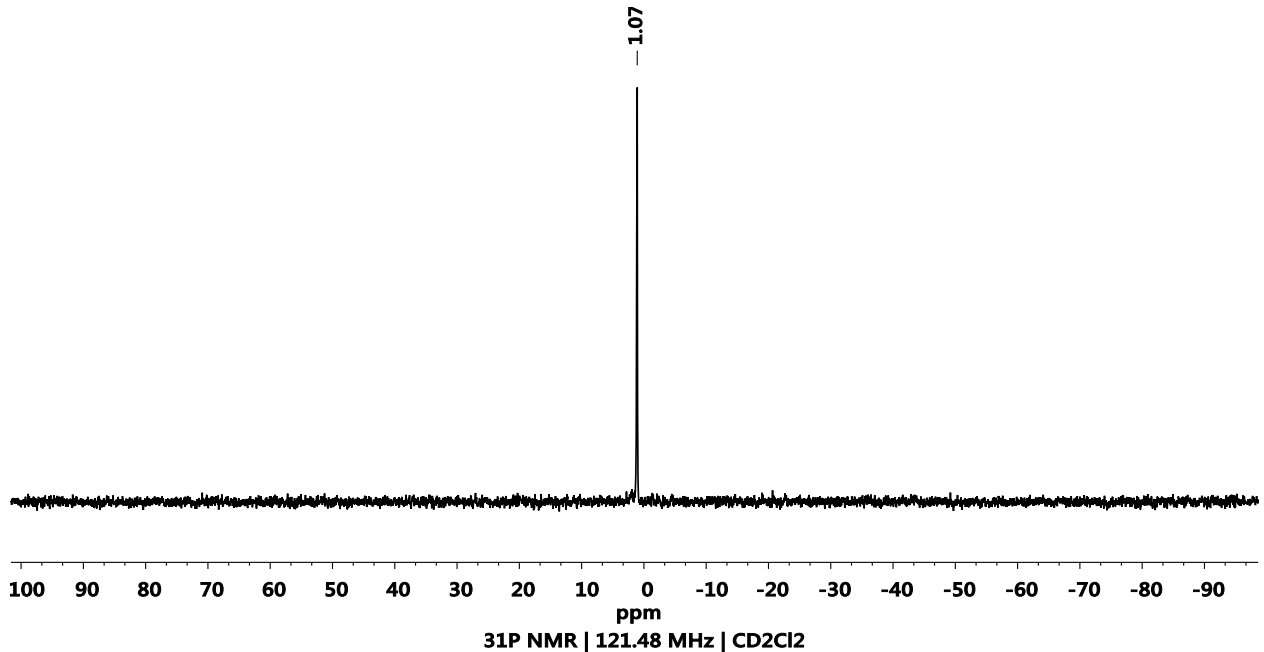


Figure S15. $^{31}\text{P}\{^1\text{H}\}$ NMR spectrum of $[(^{\text{Me}4}\text{PCP})\text{Ir}(\text{H})(\text{pyr})\text{CO}][\text{OTf}]$ (**4^{Me}**) in CD_2Cl_2 . $^{31}\text{P}\{^1\text{H}\}$ NMR (121 MHz, CD_2Cl_2): 1.07 (s).

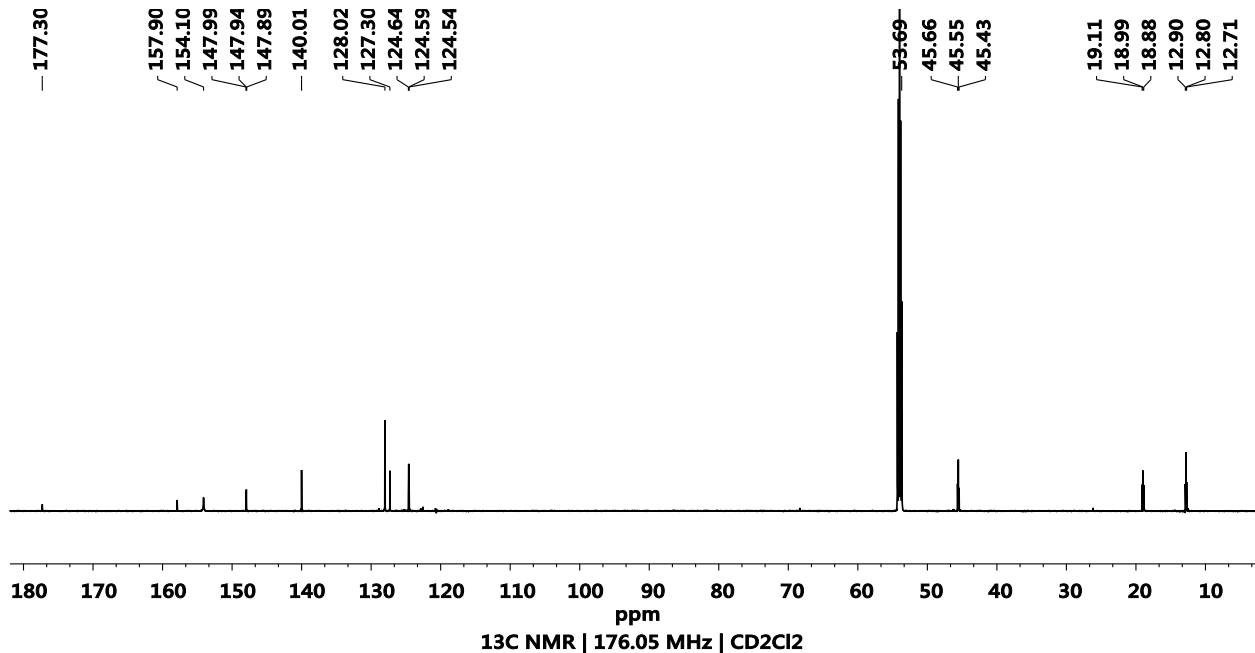
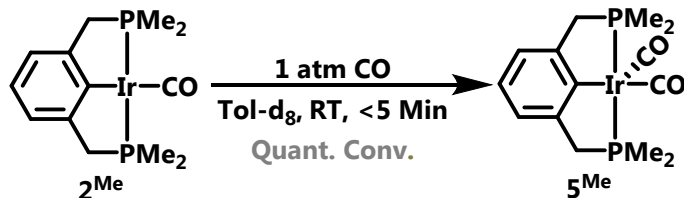


Figure S16. $^{13}\text{C}\{^1\text{H}\}$ NMR spectrum of ($^{\text{Me}4}\text{PCP}$)Ir(H)(pyr)CO[OTf] (**4^{Me}**) in CD₂Cl₂. $^{13}\text{C}\{^1\text{H}\}$ NMR (176 MHz, CD₂Cl₂): δ 177.3 (s; Ir-CO), 157.9 (s; C_{Ar}), 154.1 (s; C_{Ar}), 147.9 (t; $^3J_{\text{CP}} = 7.5$ Hz; C_{Ar}), 140.1 (s; C_{Ar}), 128.0 (s; C_{Ar}), 127.3 (s; C_{Ar}), 124.6 (t; $^3J_{\text{CP}} = 8.6$ Hz; C_{Ar}), 45.5 (vt; -(CH₂)-), 19.0 (vt; P(CH₃)), 16.1 (vt; P(CH₃)).

1.5

5^{Me}: (^{Me⁴}PCP)Ir(CO)₂



5^{Me}: (^{Me⁴}PCP)Ir(CO)₂. A solution of (^{Me⁴}PCP)Ir(CO) (**2^{Me}**) (ca. 5 mg, 0.01 mmol) in toluene-d₈ (0.350 mL) was pressurized with 1 atm of CO. The solution was vigorously shaken and turned from yellow to colorless. The spectral features are consistent with assignment to **5^{Me}**. Upon removal of the solvent under vacuum, **5^{Me}** loses CO to afford **2^{Me}**. Compound **5^{Me}** does not immediately lose CO when placed under a static vacuum.

Table S8. Characterization data for **5^{Me}**.

Method	Values
¹ H NMR	7.10 – 6.98 (m; 3H; Ar-H), (300 MHz, Tol-d ₈): 3.07 (vt; 4H; Ar(-CH ₂ -)), 1.34 (vt; 12H; -P(CH ₃))
³¹ P{ ¹ H} NMR	-5.77 (s) (121 MHz, Tol-d ₈):
¹³ C{ ¹ H} NMR	186.6 (s; Ir-CO), (126 MHz, Tol-d ₈): 147.1 (t; ² J _{CP} = 7.9 Hz; C _{Ar}), 122.9 (s; C _{Ar}), 121.0 (s; C _{Ar}), 51.2 (vt; -(CH ₂)-), 18.8 (vt; P(CH ₃))
IR	v(CO) 2010, 1930 (solution, C ₆ D ₆ , cm ⁻¹)

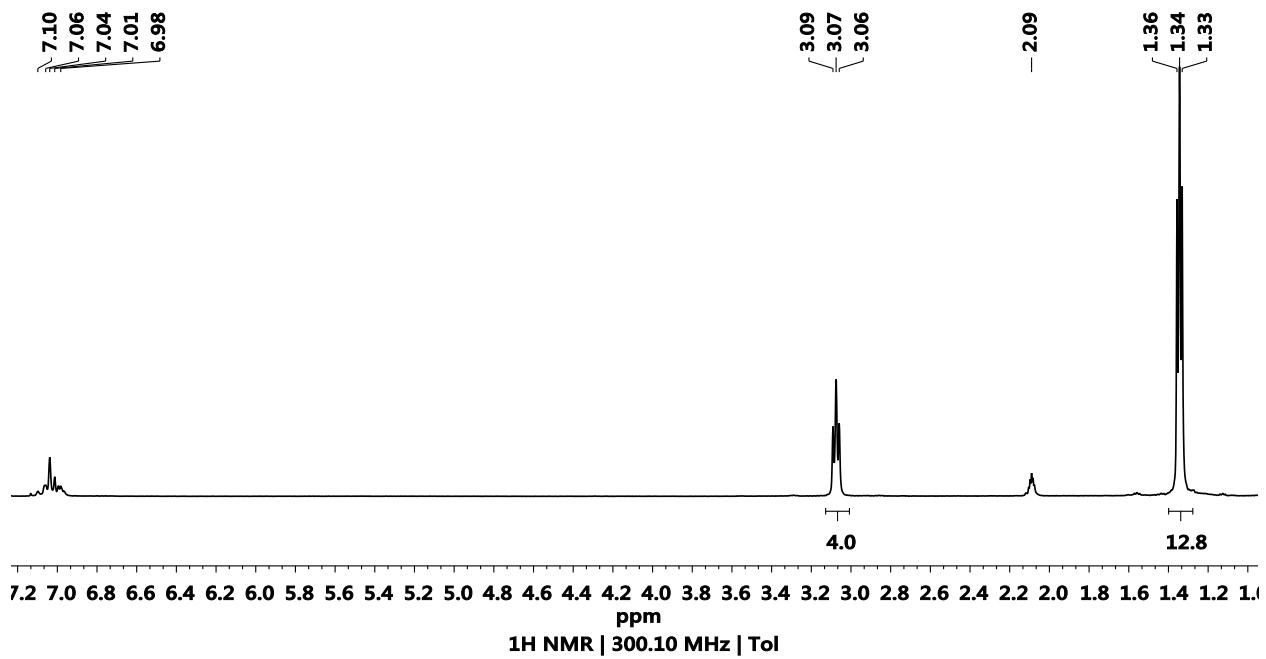


Figure S17. ^1H NMR spectrum of $(^{\text{Me}4}\text{PCP})\text{Ir}(\text{CO})_2$ (**5^{Me}**) in Tol-d_8 under 1 atm CO. ^1H NMR (300 MHz, Tol-d_8): δ 7.10 – 6.98 (m; 3H; Ar-H), 3.07 (vt; 4H, Ar(- CH_2 -)), 1.34 (vt; 12H, - $\text{P}(\text{CH}_3)$).

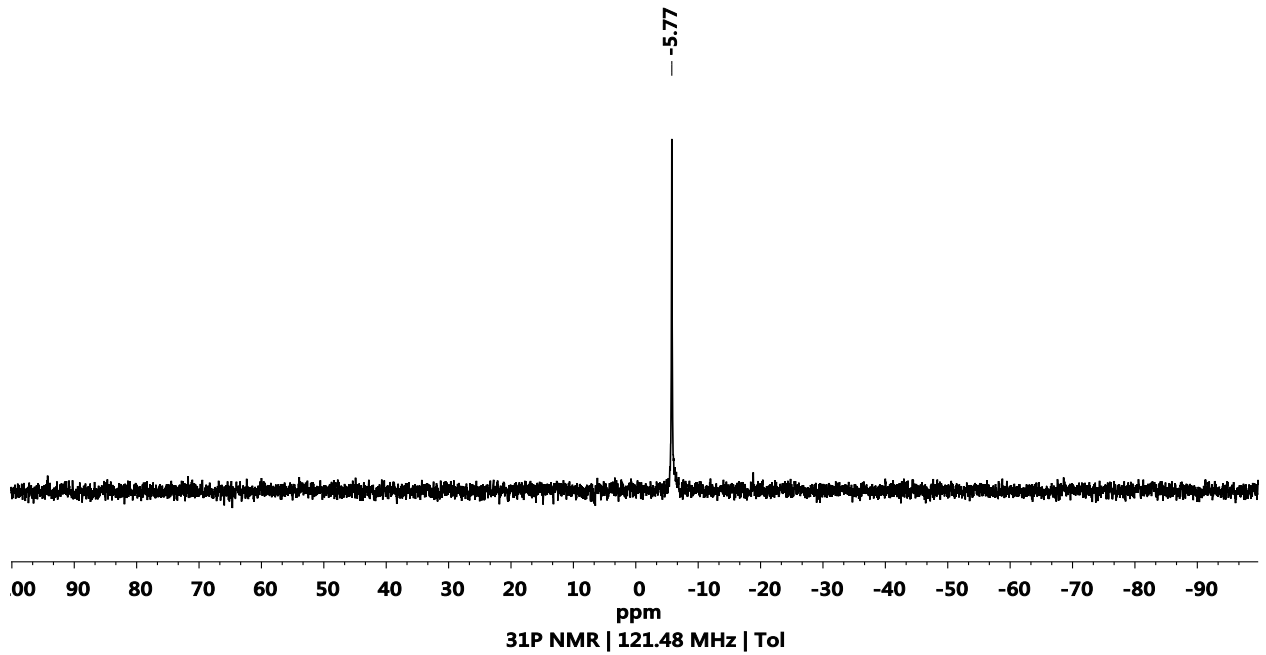


Figure S18. $^{31}\text{P}\{^1\text{H}\}$ NMR spectrum of $(^{\text{Me}4}\text{PCP})\text{Ir}(\text{CO})_2$ (**5^{Me}**) in Tol-d_8 under 1 atm CO. $^{31}\text{P}\{^1\text{H}\}$ NMR (121.5 MHz, Tol-d_8): δ -5.77.

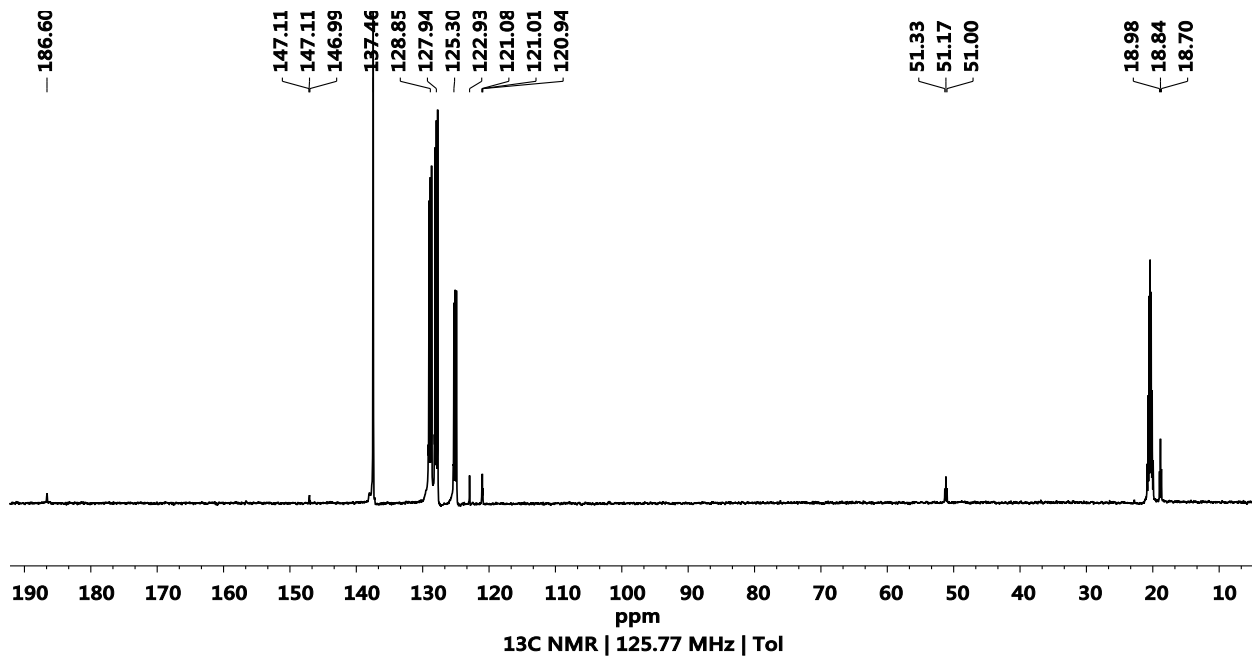


Figure S19. $^{13}\text{C}\{\text{H}\}$ NMR spectrum ($^{\text{Me}4}\text{PCP}$)Ir(CO)₂ (**5^{Me}**) in Tol-d₈ under 1 atm CO. $^{13}\text{C}\{\text{H}\}$ NMR (126 MHz, Tol-d₈): δ 186.6 (s; Ir-CO), 147.1 (t; $^2J_{\text{CP}} = 7.9$ Hz; C_{Ar}), 122.9 (s; C_{Ar}), 121.0 (s; C_{Ar}), 51.2 (vt; - (CH₂)-), 18.8 (vt; P(CH₃)).

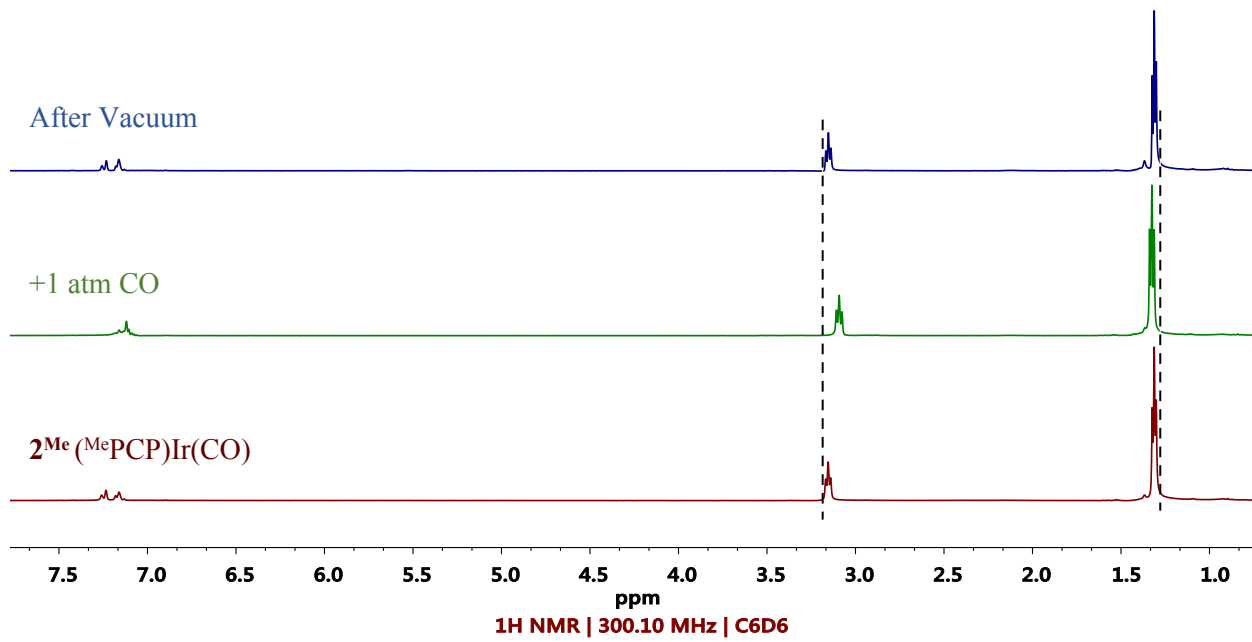
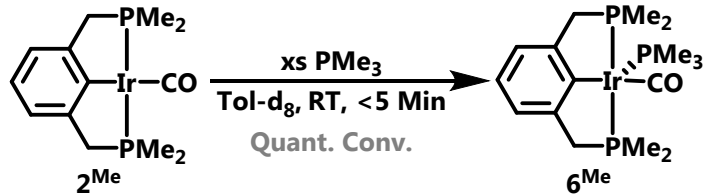


Figure S20. A comparison of the ^1H NMR spectra of ($^{\text{Me}4}\text{PCP}$)Ir(CO)₂ (**5^{Me}**) and ($^{\text{Me}}\text{PCP}$)Ir(CO) (**2^{Me}**).

1.6

6^{Me}: (^{Me⁴}PCP)Ir(CO)(PMe₃)



6^{Me}: (^{Me⁴}PCP)Ir(CO)(PMe₃). A J-Young NMR tube was charged with (^{Me⁴}PCP)Ir(CO) (ca. 5 mg, 0.01 mmol) in toluene-d₈ (0.350 mL) and PMe₃ (0.05 mL). The volatiles were removed to afford a white solid with spectroscopic features consistent with (^{Me⁴}PCP)Ir(CO)(PMe₃) (**6^{Me}**).

Table S9. Characterization data for **6^{Me}**.

Characterization	Values
¹ H NMR	7.09 (d; ³ J _{HP} = 7.3 Hz; 2H; Ar-H), (300 MHz, C ₆ D ₆): 6.98 (d; ³ J _{HP} = 7.3 Hz ;1H; Ar-H), 3.25-2.73 (br m; 4H; Ar(-CH ₂ -)), 1.60-1.37 (br m; 12H; -P(CH ₃) ₂), 1.08 (d; 9H; -P(CH ₃) ₃)
³¹ P{ ¹ H} NMR	-0.92 (d; ² J _{PP} = 112.4 Hz; 2P; -P(CH ₂)(CH ₃) ₂), (121.5 MHz, C ₆ D ₆): -55.9 (d; ² J _{PP} = 112.4 Hz; 1P; -P(CH ₃) ₃)
¹³ C{ ¹ H} NMR	192.3 (m; Ir-CO), (126 MHz, C ₆ D ₆): 146.8 (m; C _{Ar}), 128.5 (s; C _{Ar}), 121.7 (s; C _{Ar}), 121.4 (m; C _{Ar}), 52.7 (m; -(CH ₂)-), 25.7 (m; P(CH ₃) ₂), 24.4 (d; ¹ J _{PC} = 20.0 Hz P(CH ₃) ₃), 21.5 (m; P(CH ₃) ₂)
IR (solution, C ₆ D ₆ , cm ⁻¹)	v(CO) 1923

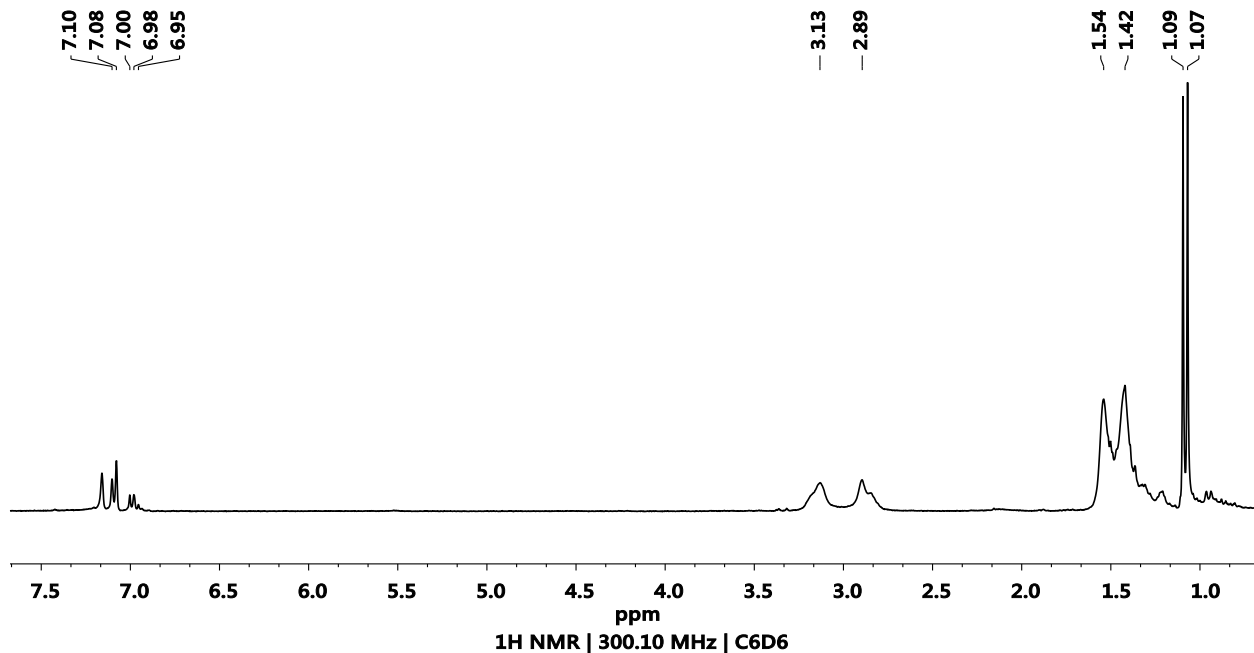


Figure S21. ^1H NMR spectrum of ($^{\text{Me}4}\text{PCP}$)Ir(CO)(PMe₃) (**6^{Me}**) in C₆D₆. ^1H NMR (300 MHz, C₆D₆): δ 7.09 (d; $^3J_{\text{HP}} = 7.3$ Hz; 2H; Ar-H), 6.98 (d; $^3J_{\text{HP}} = 7.3$ Hz; 1H; Ar-H), 3.25-2.73 (br m; 4H; Ar(-CH₂-)), 1.60-1.37 (br m; 12H; -P(CH₃)₂), 1.08 (d; 9H; -P(CH₃)₃).

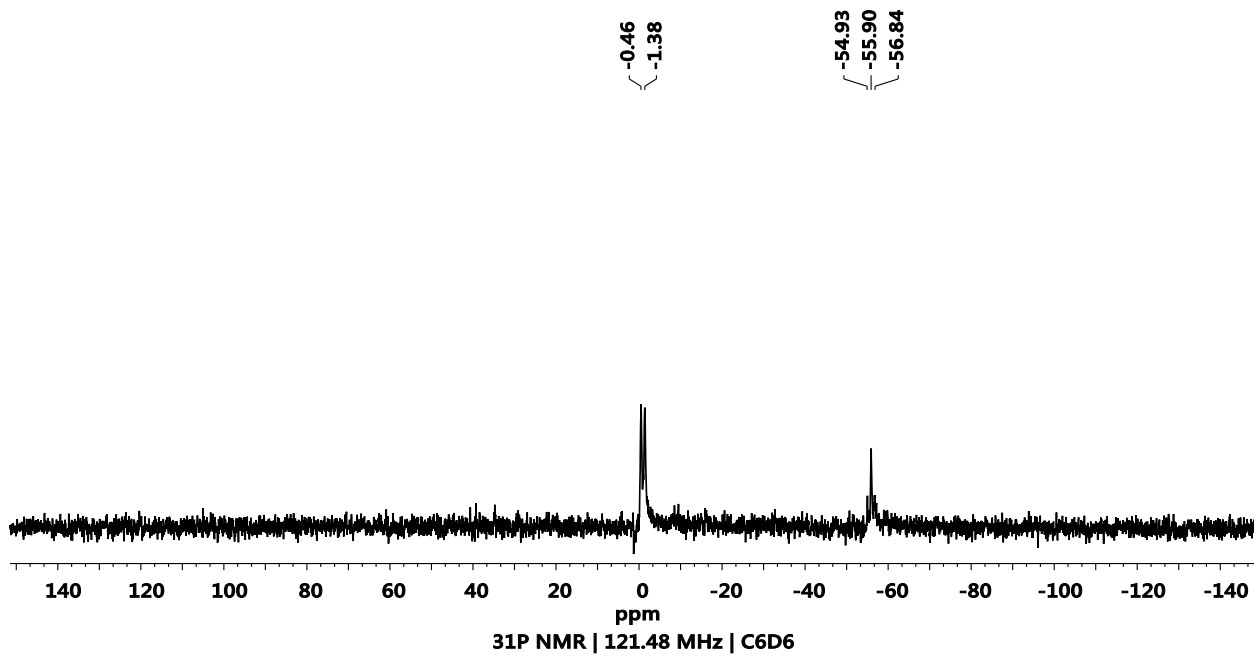


Figure S22. $^{31}\text{P}\{^1\text{H}\}$ NMR spectrum ($^{\text{Me}4}\text{PCP}$)Ir(CO)(PMe₃) (**6^{Me}**) in C₆D₆. $^{31}\text{P}\{^1\text{H}\}$ NMR (121.5 MHz, C₆D₆): δ -0.92 (d; $^2J_{\text{PP}} = 112.4$ Hz; 2P; -P(CH₂)(CH₃)₂), -55.9 (d; $^2J_{\text{PP}} = 112.4$ Hz; 1P; -P(CH₃)₃).

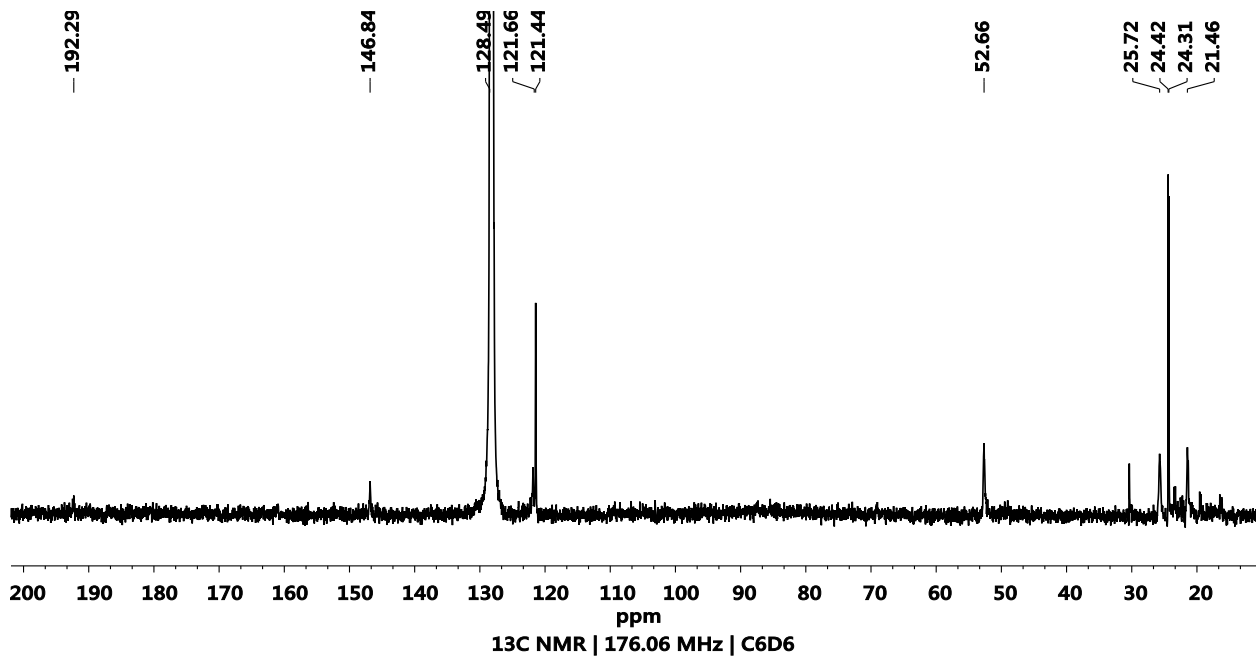
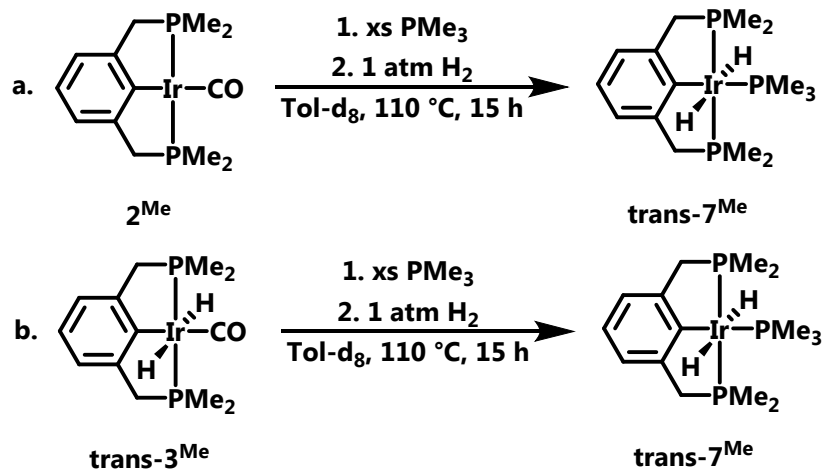


Figure S23. $^{13}\text{C}\{^1\text{H}\}$ NMR spectrum ($^{\text{Me}4}\text{PCP}$)Ir(CO)(PMe₃) (**6^{Me}**) in C₆D₆. $^{13}\text{C}\{^1\text{H}\}$ NMR (176 MHz, C₆D₆): δ 192.3 (m; Ir-CO), 146.8 (m; C_{Ar}), 128.5 (s; C_{Ar}), 121.7 (s; C_{Ar}), 121.4 (m; C_{Ar}), 52.7 (m; -(CH₂)-), 25.7 (m; P(CH₃)₂), 24.4 (d; $^1J_{\text{PC}} = 20.0$ Hz P(CH₃)₃), 21.5 (m; P(CH₃)₂).

trans-7^{Me}: (^{Me}PCP)Ir(H)₂(PMe₃)



trans-7^{Me}: trans-(^{Me}PCP)Ir(H)₂(PMe₃). Method A. A J-Young NMR tube was charged with (^{Me}PCP)Ir(CO) (**24^{Me}**) (5.2 mg, 0.01 mmol), toluene-d₈, PMe₃ (0.01 mL, 0.1 mmol). The solution was degassed, pressurized with 1 atm H₂, then vigorously shaken for 20 seconds. The solution was heated at 110 °C overnight.

Method B. A J-Young NMR tube was charged with trans-(^{Me}PCP)Ir(H)₂(CO) (**trans-7^{Me}**) (4.5 mg, 0.01 mmol), toluene-d₈, and PMe₃ (0.01 mL, 0.1 mmol). The solution was degassed, pressurized with 1 atm H₂, then vigorously shaken for 20 seconds. The solution was heated at 110 °C overnight. Crystals suitable for X-ray diffraction were grown from an impure solution of **trans-7^{Me}** and minor side-products in benzene (1 part) layered with pentane (9 parts) at -35 °C. Spectroscopic features of the major species besides PMe₃ produced by methods A and B are congruent with the structure of **trans-7^{Me}**.

Table S10. Characterization data for **trans-7^{Me}**.

Characterization	Values
¹ H NMR (300 MHz, Tol-d ₈):	δ 7.16 (m; 1H; Ar-H), 7.05 (m; 2H; Ar-H), 3.41 (vt; 4H; Ar(-CH ₂ -)), 1.56-1.51 (m; 21H; -P(CH ₃)), -10.8 (app q; ² J _{HP} = 17.1 Hz 2H; Ir-H)
³¹ P{ ¹ H} NMR (121 MHz, Tol-d ₈):	δ 1.54 (d; ² J _{PP} = 20.5 Hz), -44.7 (t; ² J _{PP} = 20.5 Hz).

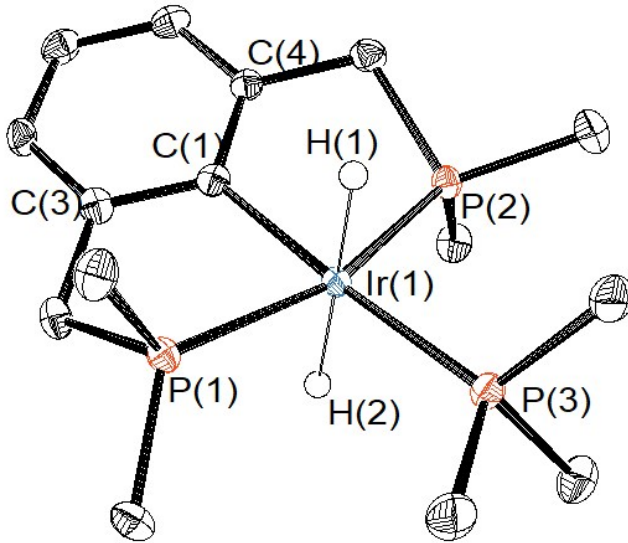


Figure S24. ORTEP⁴ of $\text{trans-}(\text{Me}_4\text{PCP})\text{Ir}(\text{H})_2(\text{PMe}_3)$ (**trans-7^{Me}**) shown with thermal ellipsoids at 50% probability. Hydrogen atoms, except Ir bound hydrides, are omitted for clarity.

Table S11. Selected bond lengths and angle for the crystal structure of $\text{trans-}(\text{Me}_4\text{PCP})\text{Ir}(\text{H})_2(\text{PMe}_3)$ (**trans-7^{Me}**), shown in Figure S24.

Bond (Å) or Angle (°)	Value
Ir(1)-C(1)	2.101(3) Å
Ir(1)-P(3)	2.2866(9) Å
Ir(I)-P(1)	2.2633 (18) Å
Ir(I)-P(2)	2.2664 (8) Å
P(1)-Ir(1)-P(2)	159.70(3) °
C(3)-C(1)-Ir(1)-P(1)	176.17(9) °
C(4)-C(1)-Ir(1)-P(2)	13.6(3) °
C(4)-C(1)-Ir(1)-P(2)	19.5(2) °

2^{iPr}: (iPr₄PCP)Ir(CO). Compound **2^{iPr}** was synthesized as previously described.³ Crystals suitable for X-ray diffraction were grown from a concentrated solution of **2^{iPr}** in pentane at -30 °C.

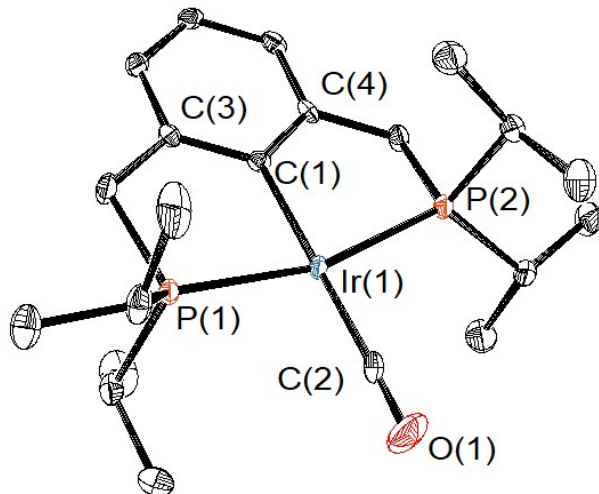


Figure S25. ORTEP⁴ of (iPr₄PCP)Ir(CO) (**2^{iPr}**) shown with thermal ellipsoids at 50% probability. Hydrogen atoms are omitted for clarity.

Table S12. Selected bond lengths and angle for the crystal structure of (iPr₄PCP)Ir(CO) (**2^{iPr}**), shown in Figure S25.

Bond (Å) or Angle (°)	Value
Ir(1)-C(1)	2.096(4) Å
Ir(1)-C(2)	1.849(4) Å
Ir(1)-O(1)	3.008(4) Å
Ir(I)-P(1)	2.2899(12) Å
Ir(I)-P(2)	2.2773(12) Å
P(1)-Ir(1)-P(2)	163.71(4) °
C(1)-Ir(1)-C(2)	178.03(17) °
C(4)-C(1)-Ir(1)-P(2)	8.0(3) °
C(4)-C(1)-Ir(1)-P(2)	10.4(3) °

trans-3^{tBu}: **trans-(^{tBu}₄PCP)Ir(H)₂(CO).** Compound **trans-3^{tBu}** was synthesized as previously described.³ Crystals suitable for X-ray diffraction were grown from a concentrated solution of **trans-3^{tBu}** in pentane at -30 °C.

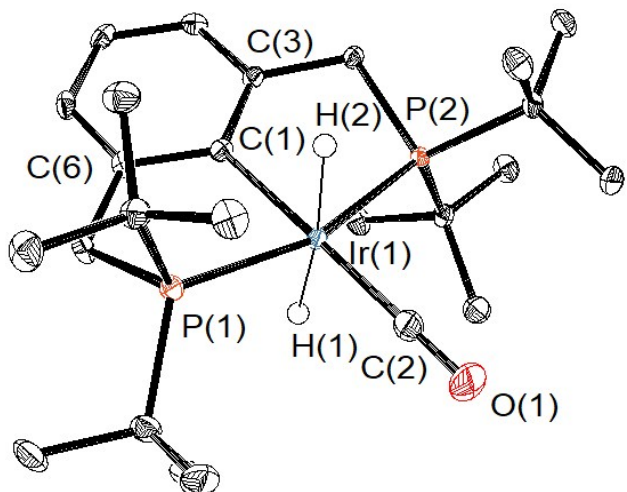


Figure S26. ORTEP⁴ of **trans-(^{tBu}₄PCP)Ir(H)₂(CO)** (**trans-3^{tBu}**) shown with thermal ellipsoids at 50% probability. Hydrogen atoms, except Ir bound hydrides, are omitted for clarity.

Table S13. Selected bond lengths and angle for the crystal structure of **trans-(^{tBu}₄PCP)Ir(H)₂(CO)** (**trans-3^{tBu}**) shown in Figure S26.

Bond (Å) or Angle (°)	Value
Ir(1)-C(1)	2.101(3) Å
Ir(1)-C(2)	1.887(3) Å
Ir(1)-O(1)	3.033(2) Å
Ir(I)-P(1)	2.3156(7) Å
Ir(I)-P(2)	2.3167(7) Å
P(1)-Ir(1)-P(2)	162.54(4) °
C(1)-Ir(1)-C(2)	178.52(11) °
C(4)-C(1)-Ir(1)-P(2)	12.3(2) °
C(4)-C(1)-Ir(1)-P(2)	13.4(2) °

2. Attempts to Trap an Intermediate During *cis/trans*-**3^{Me}** Isomerization.

Table S14. Summary of attempts to trap an intermediate.^a

Exp #	Starting	Reactant	Result
1 ^{b,d}	cis-3^{Me}	Excess PMe ₃	H ₂ Loss; 6^{Me}
2 ^{b,d}	cis-3^{Me}	^t Bu'isonitrile	Intractable
3 ^c	trans-3^{Me}	Excess PMe ₃	trans-7^{Me}
4 ^c	trans-3^{Me}	^t Bu'isonitrile	Intractable
5 ^c	5^{Me}	-	trans-3^{Me}
6 ^c	6^{Me}	-	trans-7^{Me}

^aAll reactions were conducted under 1 atm H₂. ^bRoom temperature. ^c80 °C. ^d**cis-3^{Me}** was formed *in situ*.

2.0 General Procedure for Experiments 1 and 2. A J-Young tube was charged with **2^{Me}** (ca. 5 mg, 0.01 mmol) and toluene-d₈ (350 μL). The solution was degassed, then introduced to 1 atm H₂. The J-Young tube was vigorously shaken for 20 seconds, then the reactant was introduced by syringe under a flow of H₂. The J-Young tube was vigorously shaken for 20 seconds, and then the reaction was monitored periodically by ¹H and ³¹P{¹H} NMR spectroscopy.

2.1 General Procedure for Experiments 3 and 4. A J-Young tube was charged with **trans-3^{Me}** (ca. 5 mg, 0.01 mmol), toluene-d₈ (350 μL), and the reactant. The solution was degassed, then introduced to 1 atm H₂. The J-Young tube was vigorously shaken for 20 seconds then placed into an 80 °C oil bath. The was monitored periodically by ¹H and ³¹P{¹H} NMR spectroscopy.

2.2 General Procedure for Experiments 5 and 6. A J-Young tube was charged with **5^{Me}** or **6^{Me}** (ca. 5 mg, 0.01 mmol) and toluene-d₈ (350 μL). The solution was degassed, then introduced to 1 atm H₂. The J-Young tube was vigorously shaken for 20 seconds then placed into an 80 °C oil bath. The reaction was monitored periodically by ¹H and ³¹P{¹H} NMR spectroscopy.

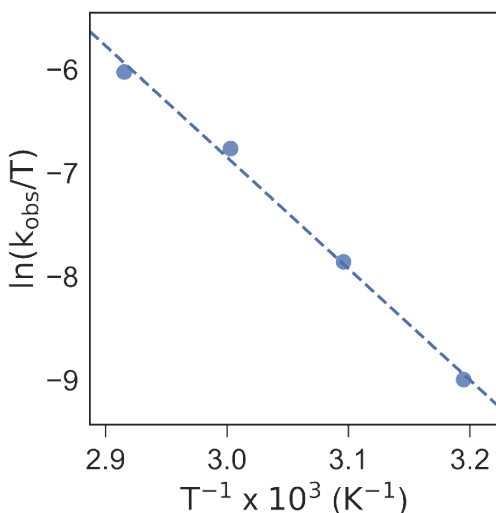
3. Kinetic Analysis of **cis**-3^{Me} to **trans**-3^{Me} under 1 atm H₂.

3.0 Kinetics Summary

Table S15. Kinetics Summary

Additive	Temperature (°C)	Rate (s ⁻¹ × 10 ³)	R ²
None	40	0.116	0.998
None	50	0.402	0.998
None	60	1.162	0.995
None	70	2.443	0.999
Pyr (8 eq)	40	0.134	0.996
NaBF ₄	40	0.326	0.991

3.1 Eyring Analysis



Thermodynamic Values

ΔH [‡]	21.2 ± 1.3 (kcal•mol ⁻¹)
ΔS [‡]	-8.84 ± 3.9 (cal•mol ⁻¹)
ΔG [‡] ₂₇₃	23.6 ± 2.2 (kcal•mol ⁻¹)

Figure S27. The Eyring plot and thermodynamic values for the isomerization of **cis**-3^{Me} to **trans**-3^{Me} under 1 atm H₂.

3.1 Kinetics General Experimental

A J-Young NMR tube was charged with (^{Me⁴}PCP)Ir(CO) **2^{Me}**, 1,3,5-Trimethoxybenzene, an optional additive and toluene-d₈. The solution was degassed, then filled with 1 atm of H₂ at room temperature. The reaction was monitored by ¹H NMR spectroscopy while the instrument was heated at the given temperature. The order of the reaction was determined by residual analysis of the linear regression fits of the zeroth, first, and second order plots using the concentration of cis-(^{Me⁴}PCP)Ir(H)₂(CO) **cis**-3^{Me}.

The reaction rates were determined by the slope of the linear regression fit of the first order plot of the concentration of cis-(^{Me}₄PCP)Ir(H)₂(CO) **cis-3^{Me}**.

3.3 Order Determination / Regression Analysis

3.3.0 Cis/Trans Equilibrium at 40 °C.

3.3.0.0 40°C. 0th Order.

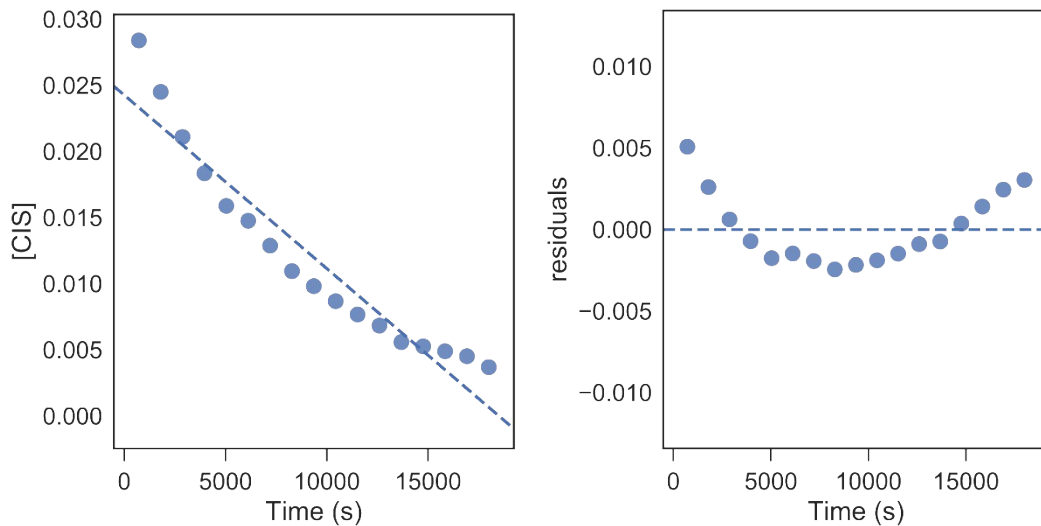


Figure S28. *Left:* Concentration of **cis-3^{Me}** vs time at 40 °C. *Right:* Residuals from the linear fit of the graph to the left vs time.

3.3.0.1 40°C. 1st Order.

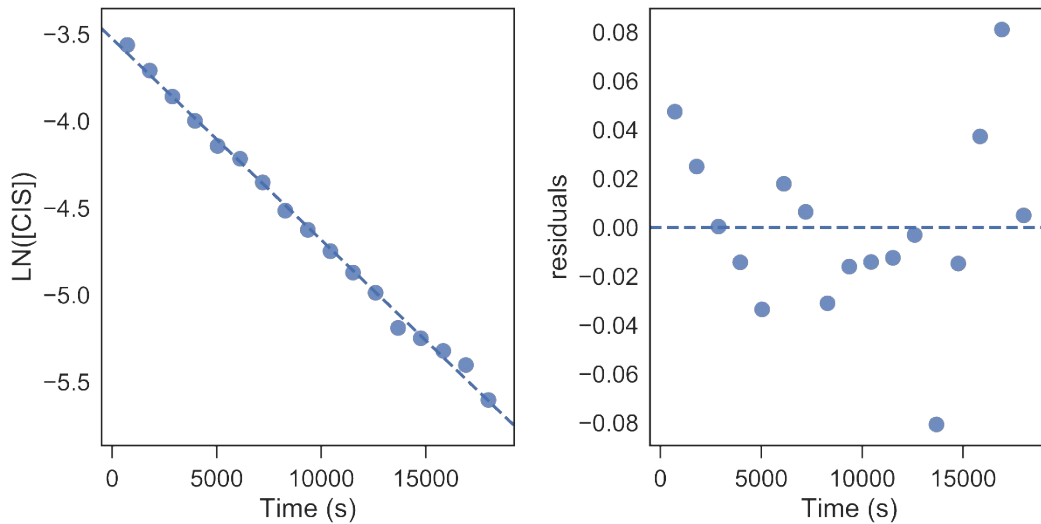


Figure S29. *Left:* Natural log of the concentration of **cis-3^{Me}** vs time at 40 °C. *Right:* Residuals from the linear fit of the graph to the left vs time.

3.3.0.2 40°C. 2nd Order.

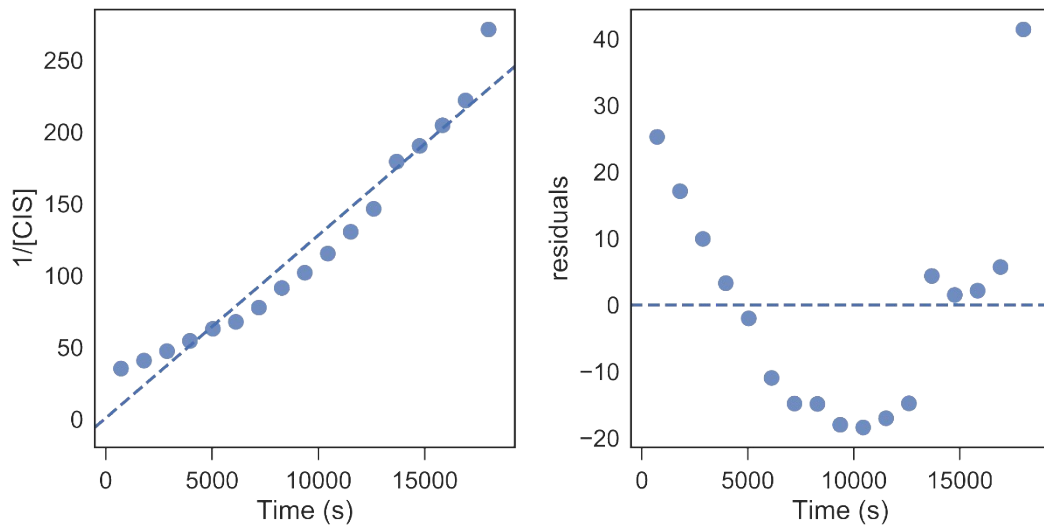


Figure S30. *Left:* Inverse of the concentration of **cis**-3^{Me} vs time at 40 °C. *Right:* Residuals from the linear fit of the graph to the left vs time.

3.3.1 Cis/Trans Equilibrium at 50 °C.

3.3.1.0 50°C. 0th Order.

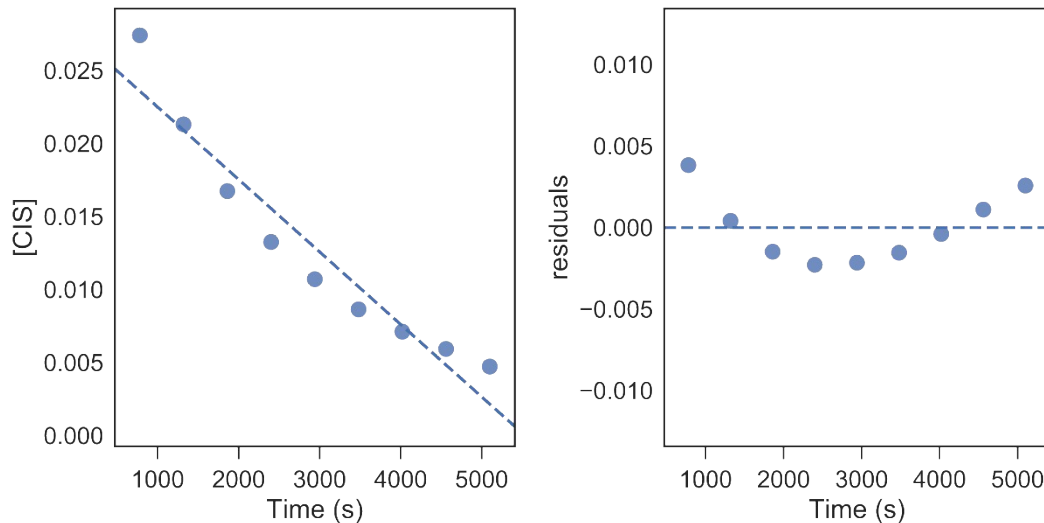


Figure S31. *Left:* Concentration of **cis**-3^{Me} vs time at 50 °C. *Right:* Residuals from the linear fit of the graph to the left vs time.

3.3.1.1 50°C. 1st Order.

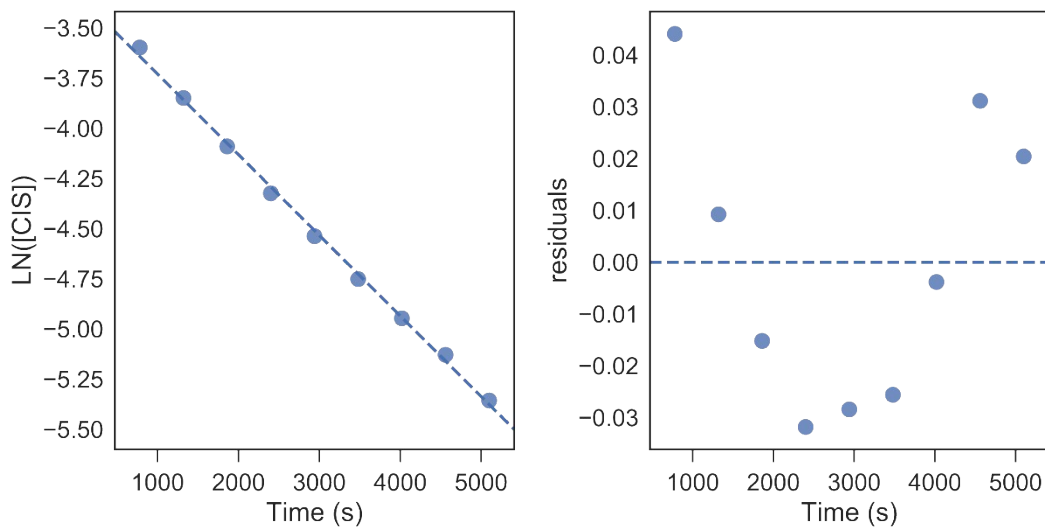


Figure S32. *Left:* Natural log of the concentration of **cis**-3^{Me} vs time at 50 °C. *Right:* Residuals from the linear fit of the graph to the left vs time.

3.3.1.2 50°C. 2nd Order.

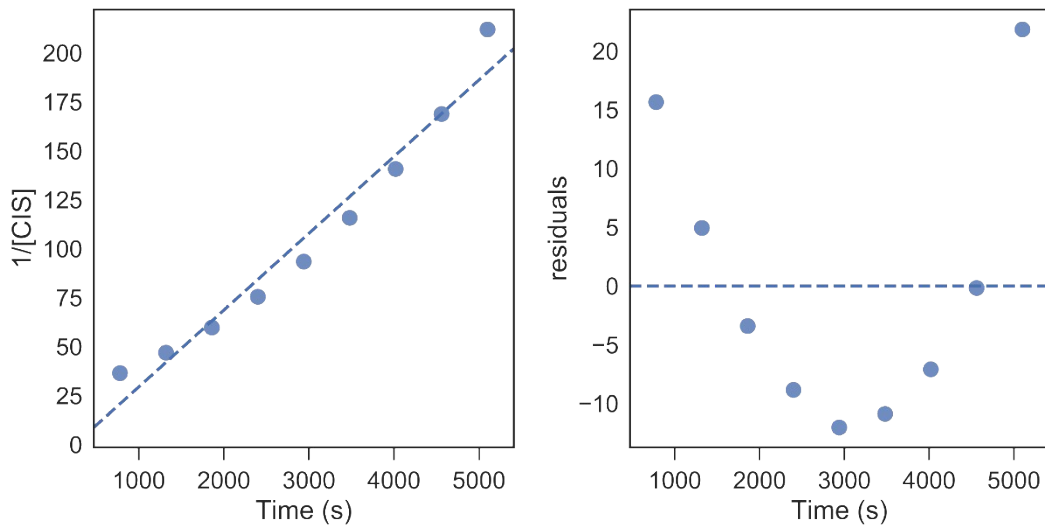


Figure S33. *Left:* Inverse of the concentration of **cis**-3^{Me} vs time at 50 °C. *Right:* Residuals from the linear fit of the graph to the left vs time.

3.3.2 Cis/Trans Equilibrium at 60 °C.

3.3.2.0 60°C. 0th Order.

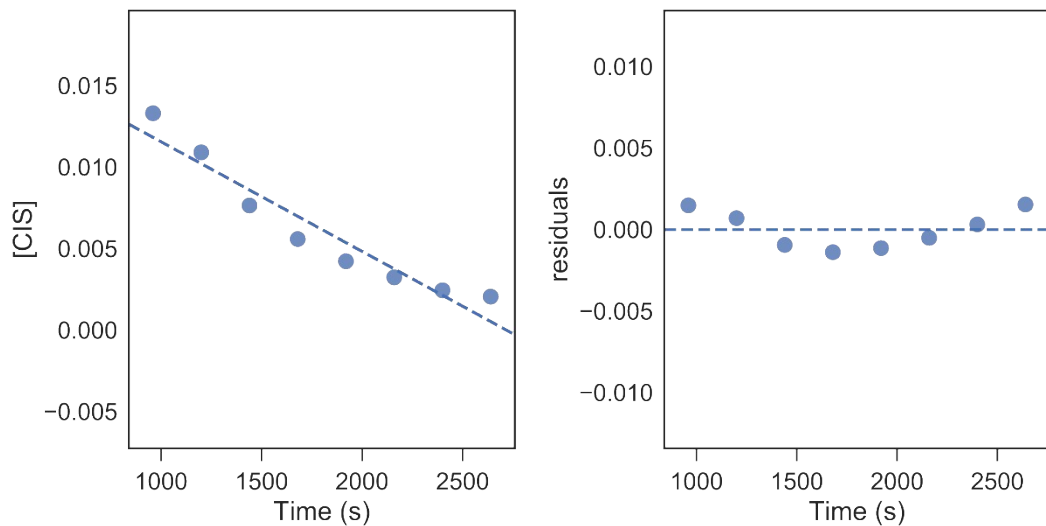


Figure S34. *Left:* Concentration of **cis-3^{Me}** vs time at 60 °C. *Right:* Residuals from the linear fit of the graph to the left vs time.

3.3.2.1 60°C. 1st Order.

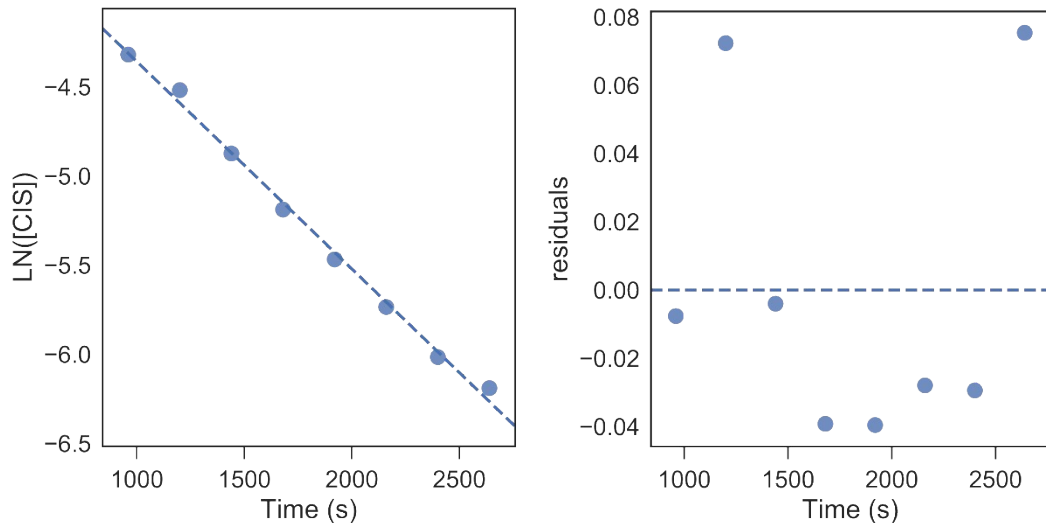


Figure S35. *Left:* Natural log of the concentration of **cis-3^{Me}** vs time at 60 °C. *Right:* Residuals from the linear fit of the graph to the left vs time.

3.3.2.2 60°C. 2nd Order.

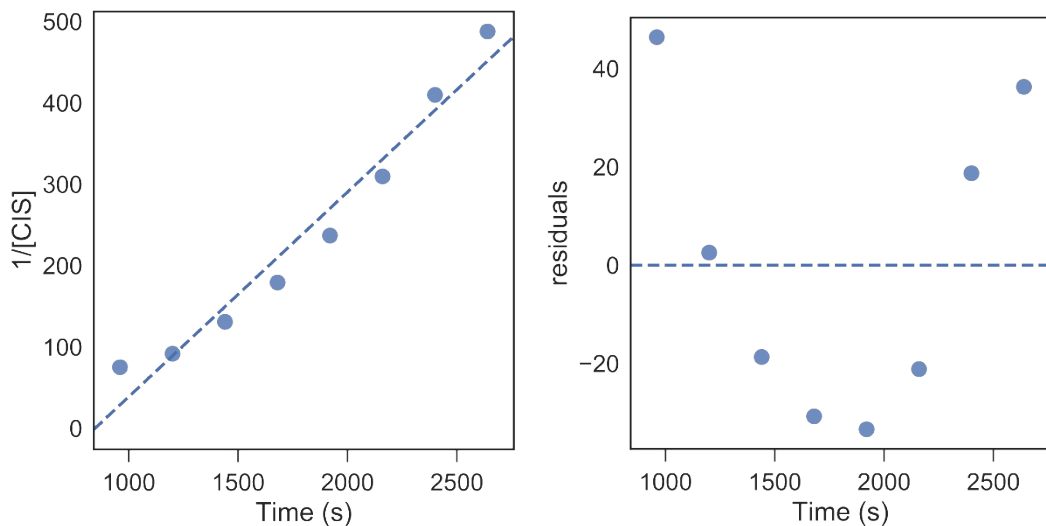


Figure S36. *Left:* Inverse of the concentration of **cis-3Me** vs time at 60 °C. *Right:* Residuals from the linear fit of the graph to the left vs time.

3.3.3 Cis/Trans Equilibrium at 70 °C.

3.3.3.0 70 °C. 0th Order.

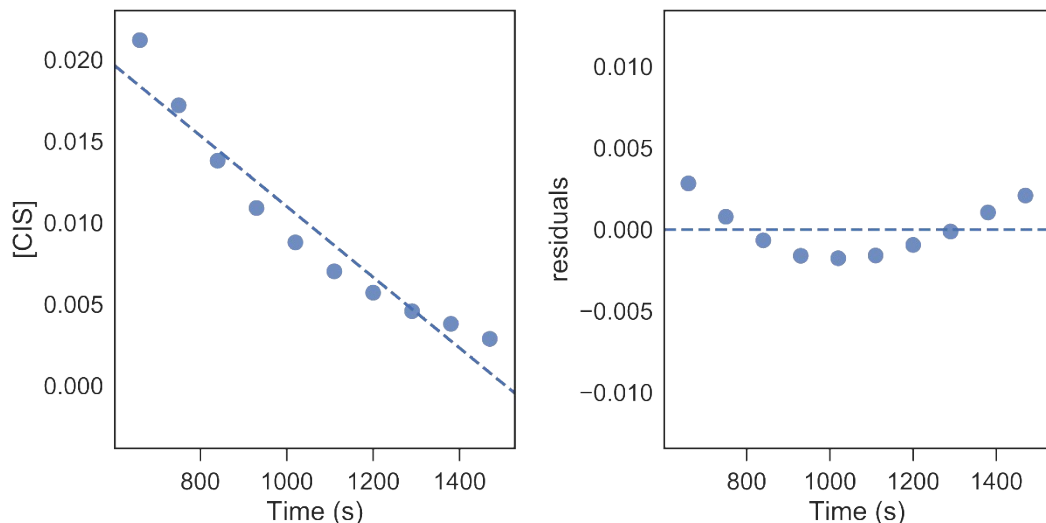


Figure S37. *Left:* Concentration of **cis-3Me** vs time at 70 °C. *Right:* Residuals from the linear fit of the graph to the left vs time.

3.3.3.1 70 °C. 1st Order.

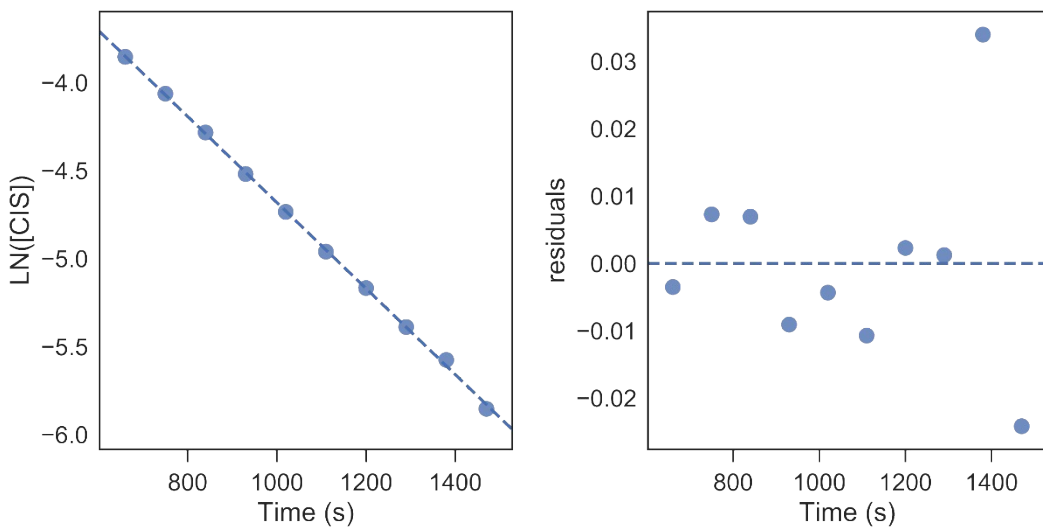


Figure S38. *Left:* Natural log of the concentration of **cis-3^{Me}** vs time at 70 °C. *Right:* Residuals from the linear fit of the graph to the left vs time.

3.3.3.2 70 °C. 2nd Order.

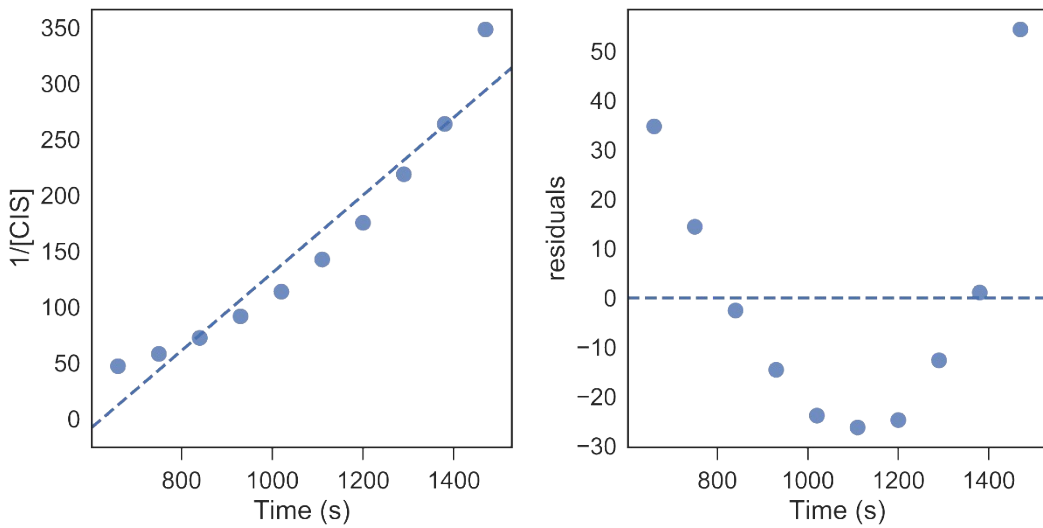


Figure S39. *Left:* Inverse of the concentration of **cis-3^{Me}** vs time at 70 °C. *Right:* Residuals from the linear fit of the graph to the left vs time.

3.3.4 Cis/Trans Equilibrium at 40 °C. 8 eq Pyridine

3.3.4.0 8 eq Pyridine. 40 °C. 0th Order.

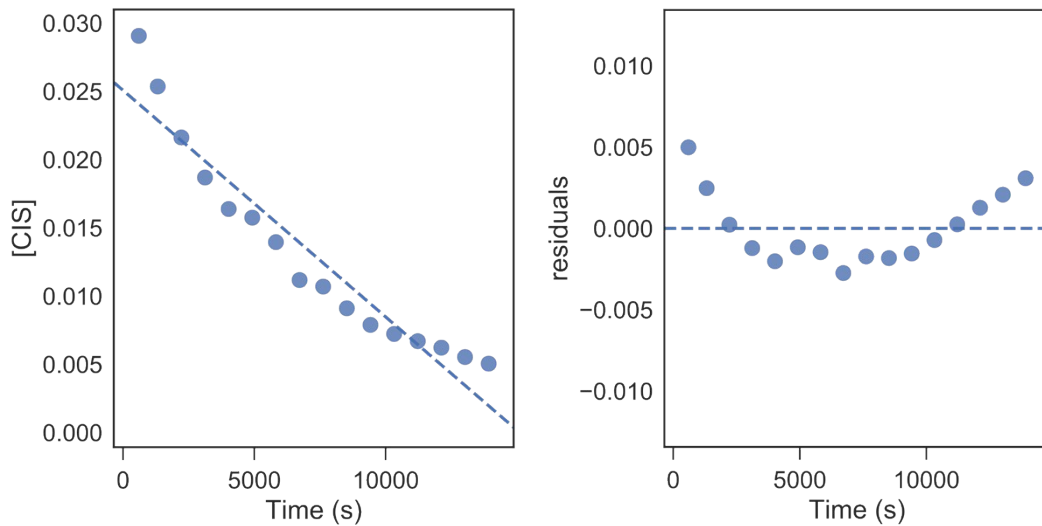


Figure S40. *Left:* Concentration of **cis-3Me** vs time at 40 °C with 8 eq pyridine. *Right:* Residuals from the linear fit of the graph to the left vs time.

3.3.4.1 8 eq Pyridine. 40 °C. 1st Order.

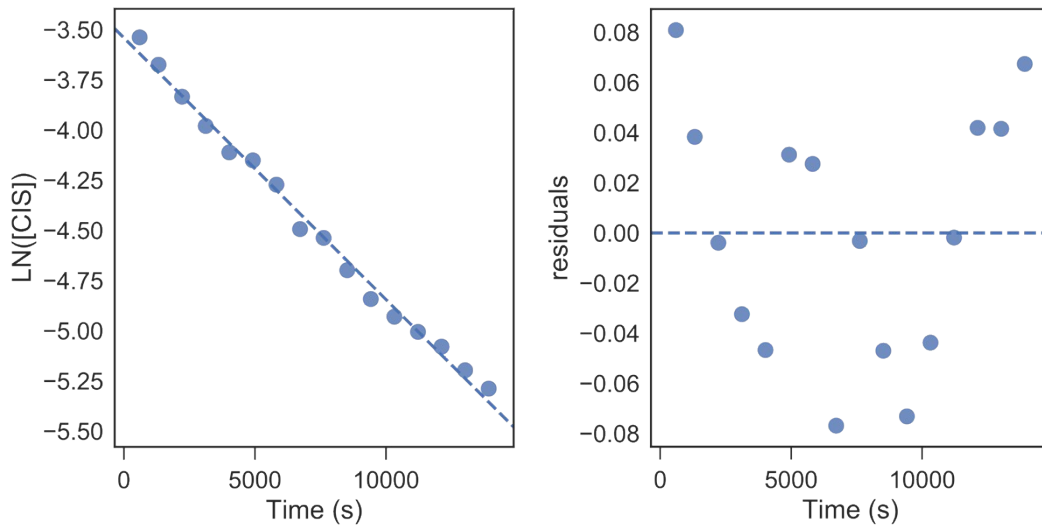


Figure S41. *Left:* Natural log of the concentration of **cis-3Me** vs time at 40 °C with 8 eq pyridine. *Right:* Residuals from the linear fit of the graph to the left vs time.

3.3.4.2 8 eq Pyridine. 40 °C. 2nd Order.

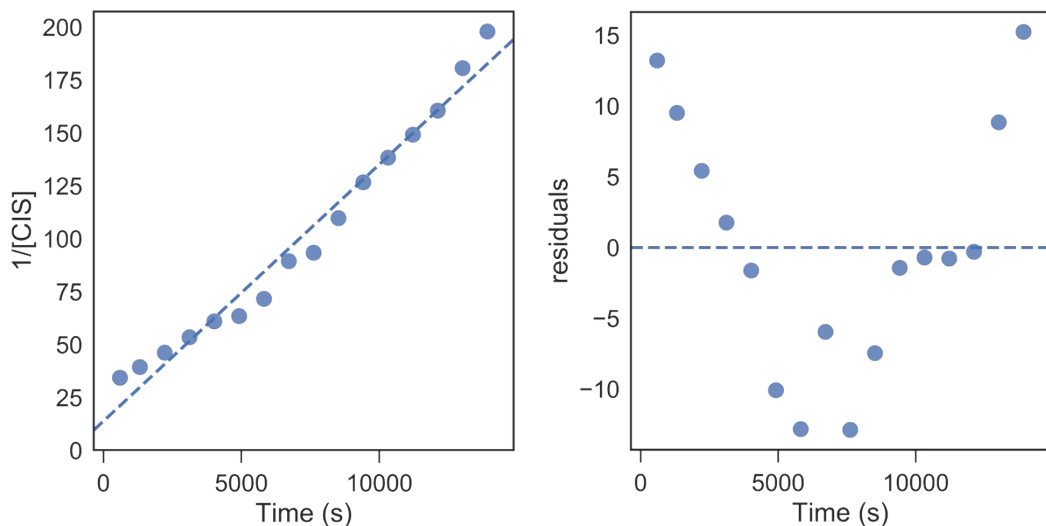


Figure S42. *Left:* Inverse of the concentration of **cis**-3^{Me} vs time at 40 °C with 8 eq pyridine. *Right:* Residuals from the linear fit of the graph to the left vs time.

3.3.5 Cis/Trans Equilibrium at 40 °C. NaBF₄.

3.3.5.0 NaBF₄. 40 °C. 0th Order.

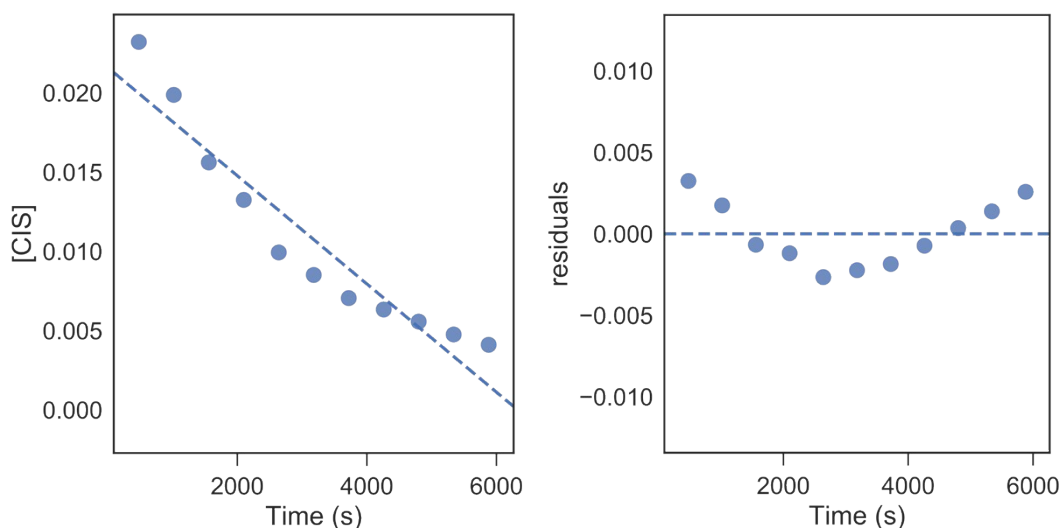


Figure S43. *Left:* Concentration of **cis**-3^{Me} vs time at 40 °C with NaBF₄. *Right:* Residuals from the linear fit of the graph to the left vs time.

3.3.5.1 NaBF₄. 40 °C. 1st Order.

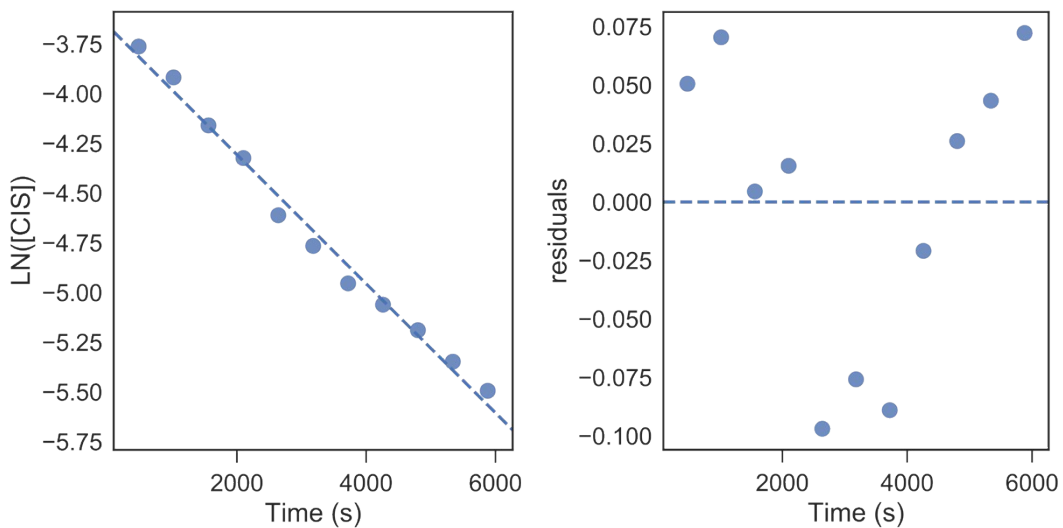


Figure S44. *Left:* Natural log of the concentration of **cis-3^{Me}** vs time at 40 °C with NaBF₄. *Right:* Residuals from the linear fit of the graph to the left vs time.

3.3.5.2 NaBF₄. 40 °C. 2nd Order.

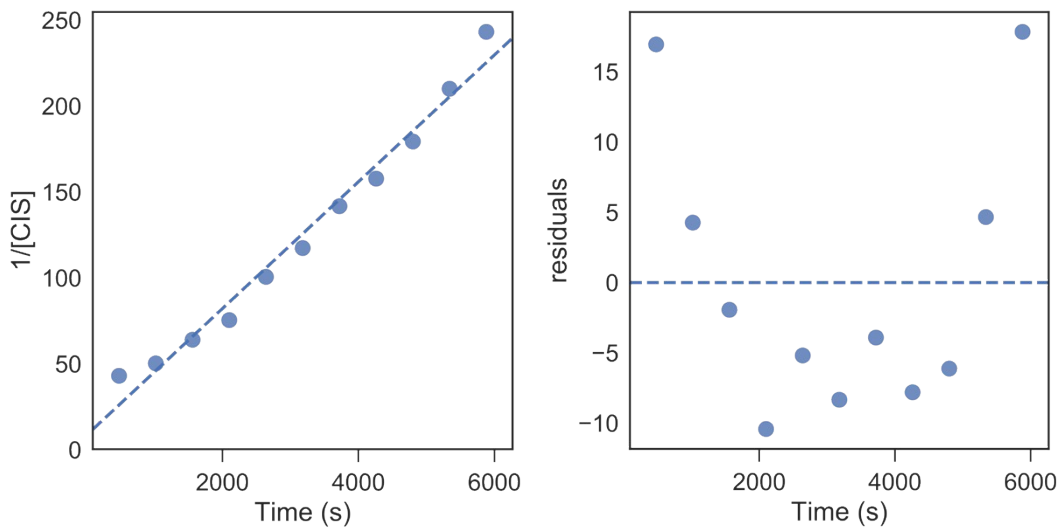


Figure S45. *Left:* Inverse of the concentration of **cis-3^{Me}** vs time at 40 °C with NaBF₄. *Right:* Residuals from the linear fit of the graph to the left vs time.

4. Crystallographic Tables and Experimental

4.0 X-ray Crystallography General Experimental

Data was collected at -173 °C on a Bruker APEX II single crystal X-ray diffractometer, Mo-radiation. The data was integrated and scaled using SAINT, SADABS within the APEX2 software package by Bruker.⁵ Solution by direct methods (SHELXS, SIR97⁶) produced a complete heavy atom phasing model consistent with the proposed structure.^{7,8} The structure was completed by difference Fourier synthesis with SHELXL97. Scattering factors are from Waasmair and Kirfel.⁹ Hydrogen atoms were placed in geometrically idealized positions and constrained to ride on their parent atoms with C---H distances in the range 0.95-1.00 Å. The hydrides are freely positionally refined with their isotropic displacement parameter 1.2 times that of the iridium. Isotropic thermal parameters U_{eq} were fixed such that they were 1.2 U_{eq} of their parent atom U_{eq} for CHs and 1.5 U_{eq} of their parent atom U_{eq} in case of methyl groups. All non-hydrogen atoms were refined anisotropically by full-matrix least-squares. Specific parameters for each crystal are described by Tables S16 and S17.

Table S16 X-ray Crystallography parameters for compounds **2^{Me}**, **trans-3^{Me}**, **trans-7^{Me}**.

Parameter	2^{Me}	trans-3^{Me}	trans-7^{Me}
Empirical formula	C ₁₃ H ₁₉ IrOP ₂	C ₁₃ H ₂₁ IrOP ₂	C ₁₅ H ₃₀ IrP ₃
Formula weight	445.42	447.44	495.50
Temperature	100(2) K	100(2) K	100(2) K
Wavelength	0.71073 Å	0.71073 Å	0.71073 Å
Crystal system	Monoclinic	Orthorhombic	Monoclinic
Space group	P 2 ₁ /c	P b c a	P 2 ₁ /c
a	13.5827(9) Å	10.0756(12) Å	22.1041(10) Å
b	10.6830(7) Å	12.0992(17) Å	9.3471(5) Å
c	20.4334(13) Å	25.280(4) Å	18.9388(9) Å
α	90 °	90 °	90 °
β	96.186(3) °	90 °	109.749(2) °
γ	90 °	90 °	90 °
Volume	2947.7(3) Å ³	3081.9(7) Å ³	3682.8(3) Å ³
Z	8	8	8
Density (calculated)	2.007 g cm ⁻³	1.929 g cm ⁻³	1.787 g cm ⁻³
Absorption coefficient	9.258 mm ⁻¹	8.856 mm ⁻¹	7.499 mm ⁻¹
F(000)	1696	1712	1936
Crystal size	0.360 x 0.280 x 0.100 mm ³	0.150 x 0.080 x 0.050 mm ³	0.140 x 0.130 x 0.060 mm ³
Theta range for data collection	2.005 to 25.350 °	1.611 to 25.348 °	1.958 to 28.445 °
Index ranges	-16<=h<=16, -12<=k<=12, -24<=l<=24	-12<=h<=12, -14<=k<=14, -30<=l<=30	-29<=h<=29, -12<=k<=12, -25<=l<=25
Reflections collected	20213	5174	17903
Independent reflections	5344 [R(int) = 0.0274]	2772 [R(int) = 0.0356]	9253 [R(int) = 0.0162]
Completeness to theta = 25.000 °	99.0 %	98.1 %	99.9 %
Refinement method	Full-matrix least-squares on F ²	Full-matrix least-squares on F ²	Full-matrix least-squares on F ²
Data / restraints / parameters	5344 / 0 / 295	2772 / 0 / 158	9253 / 6 / 369
Goodness-of-fit on F ²	1.158	1.077	1.008
Final R indices [I>2sigma(I)]	R ₁ = 0.0327, wR ₂ = 0.0695	R ₁ = 0.0329, wR ₂ = 0.0571	R ₁ = 0.0194, wR ₂ = 0.0434
R indices (all data)	R ₁ = 0.0388, wR ₂ = 0.0725	R ₁ = 0.0727, wR ₂ = 0.0721	R ₁ = 0.0254, wR ₂ = 0.0458
Largest diff. peak and hole	2.02 and -1.39 e. Å ⁻³	1.754 and -1.129 e. Å ⁻³	1.949 and -1.337 e. Å ⁻³

Table S17. X-ray Crystallography parameters for compounds **2^{iPr}**, **trans-3^{tBu}**.

Parameter	2^{iPr}	trans-3^{tBu}
Empirical formula	C ₄₂ H ₇₀ Ir ₂ O ₂ P ₄	C _{27.5} H ₅₁ IrOP ₂
Formula weight	1115.26	651.82
Temperature	100(2) K	100(2) K
Wavelength	0.71073 Å	0.71073 Å
Crystal system	Monoclinic	monoclinic
Space group	P2 ₁ /n	I2/a
a	11.2062(7)	12.3793(6) Å
b	14.0106(8)	14.3928(8) Å
c	28.6995(18)	32.473(2) Å
α	90 °	90 °
β	98.215(3) °	91.108(4) °
γ	90 °	90 °
Volume	4459.7(5) Å ³	5784.7(6) Å ³
Z	4	8
Density (calculated)	1.661 g cm ⁻³	1.497 g cm ⁻³
Absorption coefficient	6.138 mm ⁻¹	4.744 mm ⁻¹
F(000)	1696	2648.0
Crystal size	0.040 × 0.020 × 0.020 mm ³	0.18 × 0.15 × 0.12 mm ³
Theta range for data collection	2.868 to 56.712 °	3.096 to 56.834 °
Index ranges	-14 ≤ h ≤ 14, -18 ≤ k ≤ 18, -38 ≤ l ≤ 38	-15 ≤ h ≤ 16, -19 ≤ k ≤ 19, -43 ≤ l ≤ 43
Reflections collected	79985	24968
Independent reflections	11064 [R(int) = 0.0818]	7236 [R(int) = 0.0414]
Completeness to theta = 25.000 °	-	-
Refinement method	Full-matrix least-squares on F ²	Full-matrix least-squares on F ²
Data / restraints / parameters	11064/0/467	7236/0/306
Goodness-of-fit on F ²	0.980	1.046
Final R indices [I>2sigma(I)]	R ₁ = 0.0342, wR ₂ = 0.0719	R ₁ = 0.0217, wR ₂ = 0.0376
R indices (all data)	R ₁ = 0.0482, wR ₂ = 0.0751	R ₁ = 0.0365, wR ₂ = 0.0420
Largest diff. peak and hole	2.74/-1.97 e Å ⁻³	1.01/-0.76 e Å ⁻³

5. Computational Details

Calculations were performed with density functional theory (DFT) using the Gaussian09 software package.¹⁰ The PBE functional was used for all calculations.¹¹ Ir was described using the LANL2DZ basis set with an effective core potential.¹² A polarization function ($\zeta=0.685$) was added to Ir. All main group elements were described by the 6-311G(d,p) basis set.¹³ The complexes were optimized in the gas phase with a dispersion correction using the D2 versions of the Grimme's dispersion.¹⁴ Single point energies were calculated on the gas phase optimized structure in benzene using the smd solvation model for benzene ($\epsilon = 2.3$).¹⁵ Free energies are reported in kcal/mol at STP unless otherwise noted. Frequency calculations were performed on all stationary points to confirm the identity of a ground state or transition state.

6. References

- 1 G. R. Fulmer, A. J. M. Miller, N. H. Sherden, H. E. Gottlieb, A. Nudelman, B. M. Stoltz, J. E. Bercaw and K. I. Goldberg, *Organometallics*, 2010, **29**, 2176-2179.
- 2 T. T. Lekich, P. G. Askelson, R. K. Burdick and D. M. Heinekey, *Organometallics*, 2018, **37**, 211–213.
- 3 J. M. Goldberg, S. D. T. Cherry, L. M. Guard, W. Kaminsky, K. I. Goldberg and D. M. Heinekey, *Organometallics*, 2016, **35**, 3546–3556.
- 4 L.J. Farrugia, *J. App. Crystallogr.*, 1997, **30**, 565
- 5 Bruker (2007) APEX2 (Version 2.1-4), SAINT (version 7.34A), SADABS (version 2007/4), BrukerAXS Inc, Madison, Wisconsin, USA.
- 6 (a) A. Altomare, C. Burla, M. Camalli, G. L. Cascarano, C. Giacovazzo, A. Guagliardi, A. G. G. Moliterni, G. Polidori, R. Spagna, *J. App. Crystallogr.*, 1999, **32**, 115-119.
(b) A. Altomare, G. L. Cascarano, C. Giacovazzo, A. Guagliardi, *J. App. Crystallogr.*, 1993, **26**, 343-350.
- 7 (a) G.M. Sheldrick. (1997) SHELXL-97, Program for the Refinement of Crystal Structures. University of Göttingen, Germany. (b) G. M. Sheldrick, *Acta Cryst.* 2015, **C71**, 3-8.
- 8 S. Mackay, C. Edwards, A. Henderson, C. Gilmore, N. Stewart, K. Shankland, A. Donald, (1997) *MaXus: a computer program for the solution and refinement of crystal structures from diffraction data*. University of Glasgow, Scotland.
- 9 D. Waasmaier, A. Kirfel, *Acta Cryst. A.*, 1995, **51**, 416-430.
- 10 Gaussian 09, Revision D.01, Frisch, M. J.; Trucks, G. W.; Schlegel, H. B.; Scuseria, G. E.; Robb, M. A.; Cheeseman, J. R.; Scalmani, G.; Barone, V.; Mennucci, B.; Petersson, G. A.; Nakatsuji, H.; Caricato, M.; Li, X.; Hratchian, H. P.; Izmaylov, A. F.; Bloino, J.; Zheng, G.; Sonnenberg, J. L.; Hada, M.; Ehara, M.; Toyota, K.; Fukuda, R.; Hasegawa, J.; Ishida, M.; Nakajima, T.; Honda, Y.; Kitao, O.; Nakai, H.; Vreven, T.; Montgomery, J. A., Jr.; Peralta, J. E.; Ogliaro, F.; Bearpark, M.; Heyd, J. J.; Brothers, E.; Kudin, K. N.; Staroverov, V. N.; Kobayashi, R.; Normand, J.; Raghavachari, K.; Rendell, A.; Burant, J. C.; Iyengar, S. S.; Tomasi, J.; Cossi, M.; Rega, N.; Millam, J. M.; Klene, M.; Knox, J. E.; Cross, J. B.; Bakken, V.; Adamo, C.; Jaramillo, J.; Gomperts, R.; Stratmann, R. E.; Yazyev, O.; Austin, A. J.; Cammi, R.; Pomelli, C.; Ochterski, J. W.; Martin, R. L.; Morokuma, K.; Zakrzewski, V. G.; Voth, G. A.; Salvador, P.; Dannenberg, J. J.; Dapprich, S.; Daniels, A. D.; Farkas, Ö.; Foresman, J. B.; Ortiz, J. V.; Ciosowski, J.; Fox, D. J. Gaussian, Inc., Wallingford CT, 2009.
- 11 (a) J. P. Perdew, K. Burke, and M. Ernzerhof, *Phys. Rev. Lett.*, 1996, **77**, 3865.
(b) J. P. Perdew, K. Burke, and M. Ernzerhof, *Phys. Rev. Lett.*, 1997, **78**, 1396.
- 12 (a) P. J. Hay, and W. R. J. Wadt, *J. Chem. Phys.*, 1985, **82**, 270-83.
(b) W. R. J. Wadt, and P. J. Hay, *J. Chem. Phys.*, 1985, **82**, 284.
(c) P. J. Hay, and W. R. J. Wadt, *J. Chem. Phys.*, 1985, **82**, 299.
- 13 A. D. McLean, and G. S. Chandler, *J. Chem. Phys.*, 1980, **72**, 5639-48.
K. Raghavachari, J. S. Binkley, R. Seeger, J. A. Pople, *J. Chem. Phys.*, 1980, **72**, 650-54.

- 14 S. Grimme, *J. Comp. Chem.*, 2006, **27**, 1787.
- 15 A. V. Marenich, C. J. Cramer, D. G. Truhlar, *J. Phys. Chem. B*, 2009, **113**, 6378-6396.